Phage-induced efflux down-regulation boosts antibiotic efficacy

Samuel Kraus[1], Urszula Łapińska[1], Krina Chawla[1], Evan Baker[2,3], Erin L Attrill[1], Paul O'Neill[4], Audrey Farbos[4], Aaron Jeffries[4], Edouard E. Galyov[5], Sunee Korbsrisate[6], Kay B. Barnes[7], Sarah V Harding[7], Krasimira Tsaneva-Atanasova[2,3], Mark A T Blaskovich[8], Stefano Pagliara[1,9*]

[1]Living Systems Institute and Biosciences, University of Exeter, Exeter, Devon, EX4 4QD, United Kingdom
[2]Department of Mathematics and Living Systems Institute, University of Exeter, Exeter, Devon, EX4 4QD, United Kingdom
[3]EPSRC Hub for Quantitative Modelling in Healthcare, University of Exeter, Exeter, EX4 4QJ, UK
[4]Biosciences, University of Exeter, Exeter, Devon, EX4 4QD, United Kingdom
[5]Department of Genetics and Genome Biology, University of Leicester, University Road, Leicester, LE1 7RH, United Kingdom
[6]Department of Immunology, Faculty of Medicine Siriraj Hospital, Mahidol University, Bangkok 10700, Thailand
[7]Defence Science and Technology Laboratory, Porton Down, Salisbury, Wiltshire, SP4 0JQ, United Kingdom
[8]Centre for Superbug Solutions, Institute for Molecular Bioscience, The University of Queensland, St. Lucia, QLD, 4072, Australia
[9]Lead contact
*Correspondence: s.pagliara@exeter.ac.uk

Summary

The interactions between a virus and its host vary in space and time and are affected by the presence of molecules that alter the physiology of either the host or the virus. Determining the dynamics of these interactions is paramount for predicting the fate of bacterial and phage populations and for designing rational phage-antibiotic therapies. We study the interactions between stationary phase *Burkholderia thailandensis* and the phage ΦBp-AMP1. Although heterogeneous genetic resistance to phage rapidly emerges in *B. thailandensis*, the presence of phage enhances the efficacy of three major antibiotic classes, the quinolones, the beta-lactams and the tetracyclines, but antagonizes tetrahydrofolate synthesis inhibitors. Enhanced antibiotic efficacy is underpinned by reduced antibiotic efflux in the presence of phage. This new phage-antibiotic therapy allows for eradication of stationary phase bacteria, whilst requiring reduced antibiotic concentrations, which is crucial for treating infections in sites where it is difficult to achieve high antibiotic concentrations.

Keywords

Antimicrobial resistance; phage-antibiotic therapy; *Burkholderia thailandensis*; bacteriophage resistance; membrane transport; efflux; transcriptomics; gene expression; antibiotics; antibiotic accumulation

Introduction

Antimicrobial resistance (AMR) has a dramatic impact on global health with an estimated 5 million deaths associated with AMR in 2019 alone [1]. *Burkholderia* Bptm species cause life-threatening diseases [2,3 4–7] and are challenging to treat with currently available antibiotics as they are intrinsically resistant to aminoglycosides, macrolides and oxazolidinones due to constitutively expressed efflux pumps [8], whereas an atypical lipopolysaccharide structure [9] plays a crucial role in resistance to cationic peptides such as polymyxins [10].

Moreover, misuse and overuse of antibiotics in the food industry, animal husbandry, and medicine, as well as changes in the global environment have recently contributed to the spread of acquired genetic resistance [11]. *Burkholderia* Bptm species can acquire antibiotic resistance *in vivo* during treatment, which can be fatal if treatment is not shifted to alternative drugs in due course [12].

In order to overcome the development of resistance to antibiotic monotherapies, the deployment of two or more different antibiotics in combination therapies has shown some success in treating and preventing infections [13–15], although combination therapies against bacteria are still rare compared to treatments against other pathogens such as viruses [13–18]. Such limited use can be partly ascribed to the fact that antibiotics in conventional regimens can antagonize each other *in vitro* [19]. Therefore, several alternatives to traditional antibiotics have been explored in order to treat resistant infections, including: antibody therapy, antimicrobial peptides, probiotics, metal chelation, CRISPR-Cas9, bioengineered toxins, bacteriocins, vaccines and antibodies [20–27]. Although promising, all of these approaches are limited by the fact that these antimicrobial agents cannot change or adapt in real time.

In contrast, like bacteria, bacteriophages (i.e., viruses that infect bacteria) amplify at the site of an infection and evolve; therefore, also due to their high number and genetic variability, phage constitute a large and valuable reservoir of natural antimicrobials [28]. However, the use of phage as a monotherapy to treat bacterial infections presents several challenges, particularly narrow host range and the rapid evolution of resistance to phage [29]. As antibiotics are the current standard of care, using phage as an adjuvant to antibiotics instead of a monotherapy may be a more rational therapeutic use of phage [30]. Therefore, phage-antibiotic therapy has undergone a robust revitalization in the last seven years [28,31–33].

Increased efficacy of combination therapies has historically been attributed to an increase in phage produced from bacteria in the presence of β-lactam antibiotics, relative to production in their absence [34–36]. More recently, a variety of lytic phage was observed to form larger plaques in the presence of sublethal concentrations of β-lactam, quinolone and tetracycline antibiotics

[37–41]. This effect has been termed phage-antibiotic synergy [37] and has been linked to antibiotic-induced bacterial filamentation which accelerates phage assembly and cell lysis. However, other recent evidence suggests that phage-antibiotic synergy can be obtained independently of cell filamentation, enhancement of phage production or the strict use of lytic phage, and that temperate phage are also viable for phage-antibiotic therapy if prophages are induced by DNA damaging antibiotics [42].

Moreover, phage-antibiotic synergy has mostly been studied with only one or two concentrations of the antimicrobials, which is insufficient to predict combinatorial concentrations that are effective during treatment, leading to mixed results during phage-antibiotic therapy investigations [30,31,43–45]. Indeed, a recent study employing *Escherichia coli* and the lytic phage ϕHP3 tested several orders of magnitude of both phage and antibiotic concentrations, finding that the nature of the interaction between antibiotics and phage depended both on the type and concentration of the antibiotic and phage employed [46].

Therefore, it is imperative to discover and understand the emergence of resistance to phage as well as the nature of the interactions between phage and antibiotics in order to rationally design successful new phage-antibiotic therapy [28]. Here we test molecules representative of eight major antibiotic classes in combination with a recently discovered phage, termed ΦBp-AMP1 [47], that infects and kills *Burkholderia pseudomallei* and *Burkholderia thailandensis* [47,48]. ΦBp-AMP1 is a podovirus with a 45 nm icosahedral capsid, a 20 nm non-contractile tail and a 45 kb genome. In contrast to other *Burkholderia* phage that are strictly lytic [9,49], ΦBp-AMP1 displays a temperature-dependent switch from the temperate (at 25 °C) to the lytic cycle (at 37 °C) [47,50]. Using optically based microtiter plate assays and genomics, we studied the development of genetic resistance to ΦBp-AMP1 in stationary phase *B. thailandensis*. We investigated the dynamics of the interactions between ΦBp-AMP1 and representative molecules of the major antibiotic classes over multiple orders of magnitude of antibiotic concentrations and phage titers. We further analysed these phage-antibiotic interactions via single-cell microscopy, mathematical modelling and gene expression profiling of stationary phase *B. thailandensis* undergoing phage-antibiotic combination therapy as well as antibiotic or phage monotherapy.

Results

Genetic resistance to ΦBp-AMP1 phage in *B. thailandensis* is heterogeneous

We used well-mixed liquid cultures of stationary phase *B. thailandensis* (strain E264) with ΦBp-AMP1 at a multiplicity of infection (MOI) of 1 in lysogeny broth (LB) medium at 37 °C [51]

and performed colony forming unit (CFU) assays every 2 h over a 24 h period. For the first 14 h of incubation in the presence of phage, we did not observe neither a reduction nor an increase of the bacterial population, despite the presence of LB medium allowed regrowth of uninfected stationary phase *B. thailandensis* cultures (Figure 1A).

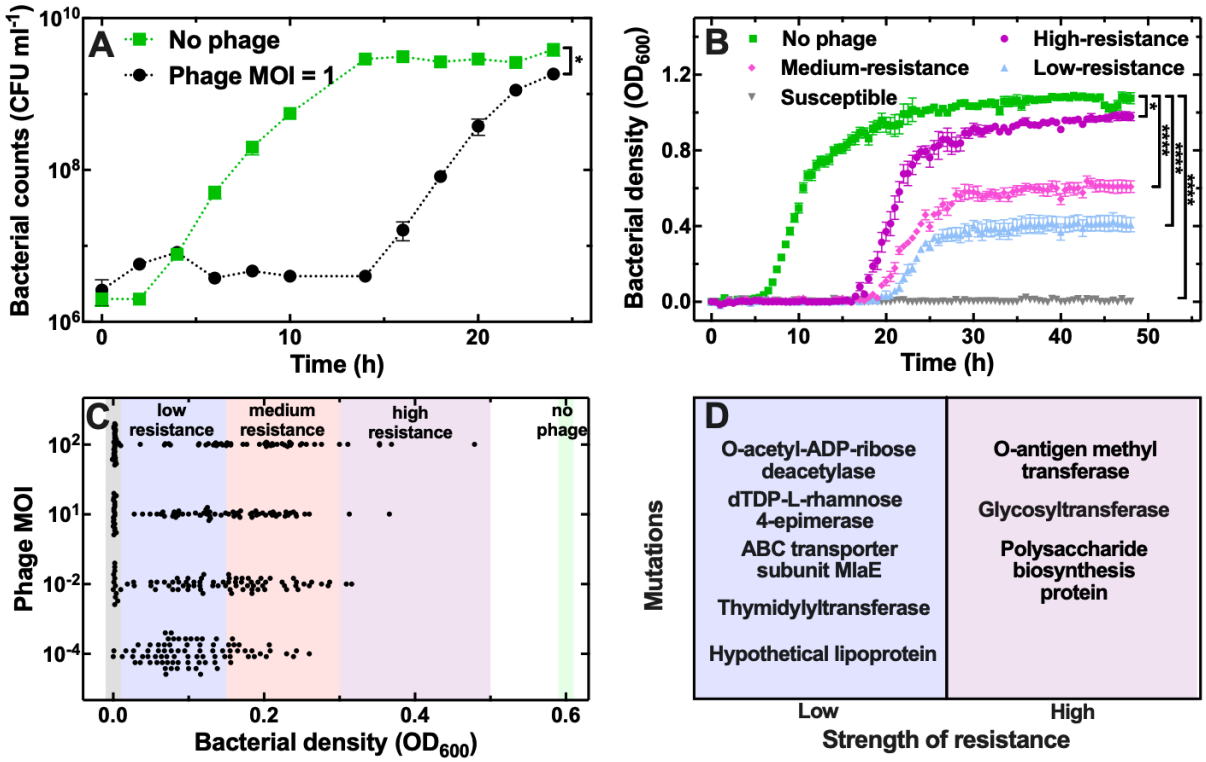

Figure 1 Heterogenous resistance to ΦBp-AMP1 in *B. thailandensis*. (A) Regrowth of stationary phase *B. thailandensis* populations in the presence of LB medium only (green squares) or together with phage at an MOI of 1 (black circles). Symbols and error bars are means and standard errors of the means of CFU measurements obtained from biological triplicates each containing technical triplicates. Very small error bars cannot be visualised due to overlap with the datapoints. Dotted lines are guides-for-the-eye. Corresponding phage counts are reported in Figure S1. (B) Regrowth of stationary phase *B. thailandensis* populations in the presence of LB medium only ($1.05 < OD_{600} < 1.2$ after 48 h, green squares) or together with phage at an MOI of 1 with different levels of bacterial resistance to phage emerging: high-resistance ($0.9 < OD_{600} < 1.05$ after 48 h, purple circles), medium-resistance ($0.5 < OD_{600} < 0.7$ after 48 h, magenta diamonds), low-resistance ($0.3 < OD_{600} < 0.5$ after 48 h, blue upward triangles), susceptible ($0 < OD_{600} < 0.01$ after 48 h, grey downward triangles). Symbols and error bars are means and standard errors of bacterial density values, measured in OD_{600}, obtained from 84 technical replicates from biological triplicates. Very small error bars cannot be visualised due to overlap with the datapoints. * indicate a p-value < 0.05, **** indicate a p-value < 0.0001. (C). Bacterial density measurements after 24 h in the presence of phage at an MOI of 10^{-4}, 10^{-2}, 1 and 10^{2}. Each black circle represents a bacterial density value performed on one of 84 technical micro-culture replicates from biological triplicates. The coloured vertical bands in the background indicate the range of OD_{600} values for each level of resistance after 24 h: high-resistance ($0.3 < OD_{600} < 0.5$, purple band), medium-resistance ($0.15 < OD_{600} < 0.3$, magenta band), low-resistance ($0.01 < OD_{600} < 0.15$, blue band), susceptibility ($0 < OD_{600} < 0.01$, grey band). (D) Unique mutations identified in five representative low- and high-resistance mutants. See Table S1 for further details.

The phage population instead increased within the first 4 h of co-incubation and reached a plateau after 6 h (Figure S1). The bacterial population started to increase after 14 h co-

137 incubation with phage and after 24 h reached a plateau 2-fold lower compared to that
138 measured in the absence of phage (Figure 1A). These data suggest that a bacterial
139 subpopulation survives phage treatment, passes on phage immunity to its progeny and
140 becomes the predominant genotype within the population; in contrast, a susceptible
141 subpopulation becomes a minority due to phage infection but persists in the presence of phage
142 since the phage population does not decline within our experimental time frame (Figure S1).

143 To test this hypothesis, we infected 84 different stationary phase bacterial micro-cultures and
144 measured the bacterial density in the presence of phage and LB medium. We found that some
145 bacterial micro-cultures contained only bacteria that were susceptible to phage and did not
146 grow; whereas in other bacterial micro-cultures genetic resistance to phage emerged and the
147 cultures started to regrow in the presence of LB medium, albeit with different onset times,
148 slopes and saturations of growth (Figure 1B). Overall, the distribution of growth levels
149 observed could be described by a hurdle-gamma distribution (Figure 1C and Figure S2),
150 where the hurdle describes the cultures that are susceptible to phage, whereas the gamma
151 describes the spread of growth in the cultures that are resistant to phage. These data suggest
152 that *B. thailandensis* populations must contain a heterogeneous pool of mutants that are
153 resistant to the phage.

154 Next, we set out to investigate whether the phage MOI has an impact on the emergence of a
155 heterogeneous pool of genetically resistant mutants. We infected 84 stationary phase bacterial
156 micro-cultures with four different phage MOIs and measured the bacterial density after 24 h.
157 We found that the proportion of cultures susceptible to phage increased with the MOI; the
158 fraction of cultures displaying low resistance to phage or high resistance to phage reduced
159 and increased, respectively, with increasing phage MOI (Figure 1C and Figure S2). Moreover,
160 all of the cultures grew when treated with ΦBp-AMP1 at an MOI of 1 at 25 °C (Figure S3),
161 confirming that ΦBp-AMP1 features a temperature-dependent switch from the lytic to the
162 lysogenic cycle.

163 To investigate the mechanisms underpinning resistance to phage, we harvested survivor
164 populations from the experiments above and inoculated them either into 96-well plates or onto
165 agar plates containing phage. We found that all survivors grew in the presence of ΦBp-AMP1
166 and LB medium, suggesting that the bacterial populations had become genetically resistant to
167 phage. However, the colonies produced by these resistant mutants were smaller compared to
168 the parental strain (Figure S4), suggesting that these mutations brought about a fitness cost
169 [32]. Therefore, we set out to understand which genetic mutations had emerged within the
170 population during phage treatment. We sequenced the genome of five representative high-
171 resistant and low-resistant survivor cultures. We found that low resistance was due to unique

172 mutations in genes encoding the O-acetyl-ADP-ribose deacetylase, the dTDP-L-rhamnose-4-
173 epimerase, the ABC transporter subunit MlaE, the thymidylyltransferase and a hypothetical
174 lipoprotein (Figure 1D and Table S1). High resistance was instead due to unique mutations of
175 three genes encoding the O-antigen methyl transferase, a glycosyltransferase and a
176 polysaccharide biosynthesis protein. Moreover, we did not find lysogenic ΦBp-AMP1 in any
177 of the genomes sequenced (Table S2), suggesting that stable lysogeny did not occur at 37
178 °C. We found two common temperate bacteriophages of *Burkholderia* species, ΦE12-2 and
179 ΦE125, in all sequenced *B. thailandensis* genomes (Table S2).

180 Taken together, these data suggest that ΦBp-AMP1 is a lytic phage of *B. thailandensis* at 37
181 °C, that different levels of genetic resistance can emerge within putatively clonal populations
182 of *B. thailandensis* depending on the phage MOI employed and that mutations of genes
183 encoding membrane associated proteins confer high resistance to ΦBp-AMP1. Therefore, in
184 order to make ΦBp-AMP1 effective in eradicating stationary phase *B. thailandensis* there is a
185 need to use this phage in combination with clinically relevant antibiotics.

186

187 **ΦBp-AMP1 phage increases the growth inhibitory efficacy of quinolones, β-lactams and**
188 **tetracyclines**

189 We set out to investigate whether the use of ΦBp-AMP1 increases the efficacy of clinically
190 relevant antibiotics in inhibiting the regrowth of stationary phase *B. thailandensis* when
191 incubated in LB medium. We used four major antibiotic classes commonly employed for
192 treatment of melioidosis, namely quinolones, β-lactams, tetracyclines and tetrahydrofolate
193 synthesis inhibitors as well as antimicrobial agents that are not routinely employed to treat
194 melioidosis, namely aminoglycosides, oxazolidinones, macrolides and glycopeptides (Table
195 1). We determined the fractional inhibitory concentration (FIC) index of each antibiotic against
196 stationary phase *B. thailandensis* by dividing the minimum inhibitory concentration (MIC) [52]
197 derived from combination therapy with phage at an MOI of 1 by the MIC of antibiotic
198 monotherapy. Therefore, the smaller the FIC index value measured, the higher is the increase
199 in antibiotic efficacy of the combination therapy.

200 Remarkably, combination therapy increased the efficacy of a diverse range of molecules
201 representative of all of the fluoroquinolone generations. Specifically, we measured an FIC
202 index of 0.25 for nalidixic acid (1st generation fluoroquinolone), 0.06 for ciprofloxacin (2nd
203 generation), 0.125 for levofloxacin (3rd generation), 0.125 for moxifloxacin (4th generation) and
204 0.03 for finafloxacin (5th generation). Similarly, combination therapy increased the efficacy of

205 representative β-lactams and tetracyclines against *B. thailandensis*; however, combination
206 therapy did not increase the efficacy of tetrahydrofolate synthesis inhibitors (Table 1).

Class	Molecule	Monotherapy MIC (μg ml^{-1})	Co-treatment MIC (μg ml^{-1})	FIC
Quinolones	Nalidixic Acid	16	4	0.25
	Ciprofloxacin	2	0.125	0.06
	Ofloxacin	4	0.5	0.125
	Levofloxacin	4	0.5	0.125
	Finafloxacin	2	0.06	0.03
	Moxifloxacin	2	0.25	0.125
β-Lactams	Amoxicillin	64	16	0.25
	Ampicillin	64	16	0.25
	Cefaclor	256	64	0.25
	Ceftazidime	2	0.25	0.125
	Meropenem	8	2	0.25
Tetracyclines	Doxycycline	4	1	0.25
	Tetracycline	8	2	0.25
Tetrahydrofolate Synthesis Inhibitors	Trimethoprim (TMP)	32	32	1
	Sulfamethoxazole (SMX)	1024	1024	1
	Co-trimoxazole (TMP/SMX)	32/160	32/160	1
Aminoglycosides	Gentamicin	>512	>512	-
	Streptomycin	>512	>512	-
Oxazolidinones	Linezolid	>512	>512	-
Macrolides	Roxithromycin	>512	>512	-
Glycopeptides	Vancomycin	>512	>512	-

207 **Table 1 ΦBp-AMP1 phage increases the inhibitory efficacy of quinolones, β-lactams and**
208 **tetracyclines.** Antibiotic class, antibiotic molecule, minimum inhibitory concentration (MIC) measured
209 against stationary phase *B. thailandensis* when used as monotherapy or in combination therapy with
210 phage ΦBp-AMP1 at an MOI of 1 and the fractional inhibitory concentration (FIC) as the ratio of the
211 MIC value obtained from the combination therapy over the MIC value obtained from monotherapy. The
212 initial bacterial inoculum was 5×10^5 cells mL^{-1}, regrowth of stationary phase bacteria was measured as
213 optical density after 24 h of monotherapy or combination therapy compared with regrowth of untreated
214 stationary phase bacteria incubated in LB medium only. The MIC value after 24 h was determined as
215 the antibiotic concentration value for which the bacterial growth was less than 10% the growth value
216 measured for untreated bacteria. Each measurement was performed in biological triplicates each
217 consisting of five technical replicates.

218

Inspired by these successful combination therapy findings, we set out to determine whether combination therapy with phage increased the efficacy of antibiotics that are not routinely employed to treat melioidosis. However, combination therapy with phage did not increase the efficacy of two aminoglycosides, an oxazolidinone, a macrolide or a glycopeptide (Table 1), antibiotics against which *B. thailandensis* is intrinsically resistant due to constitutively expressed efflux pumps [8] and an atypical lipopolysaccharide structure [53].

Next, we investigated the bacterial population dynamics in the presence of phage and a sub-inhibitory concentration of levofloxacin, cefaclor or trimethoprim for which combination therapy with phage provided high, medium or no increase in efficacy, respectively (Table 1). Combination therapy with 0.25× MIC levofloxacin and phage at an MOI of 1 in LB medium did not allow for regrowth of stationary phase *B. thailandensis* within the 24 h experimental timeframe, whereas regrowth started after 5 h exposure to levofloxacin monotherapy and 16 h after exposure to phage monotherapy (Figure 2A).

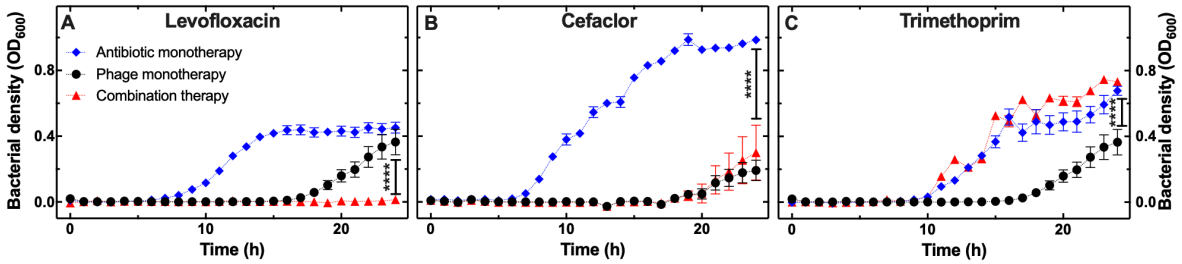

Figure 2 Bacterial population dynamics in the presence of ΦBp-AMP1 and sub-inhibitory antibiotic concentrations. Regrowth of stationary phase *B. thailandensis* populations in the presence of LB medium and either phage at an MOI of 1 (black circles), or 0.25× MIC of (A) levofloxacin, (B) cefaclor or (C) trimethoprim either as monotherapy (blue diamonds) or in combination therapy with phage at an MOI of 1 (red triangles). Symbols and error bars are means and standard errors of the means of bacterial density values, measured in OD_{600}, obtained from biological triplicates each consisting of five technical replicates. Very small error bars cannot be visualised due to overlap with the datapoints. Dotted lines are guides-for-the-eye. **** indicate a p-value < 0.0001.

Following cefaclor monotherapy at 0.25× its MIC, the stationary phase *B. thailandensis* population started to regrow after 5 h, whereas following either phage monotherapy at an MOI of 1 or combination therapy with 0.25× MIC cefaclor and phage at an MOI of 1, the stationary phase *B. thailandensis* population started to regrow after 16 h and reached a plateau that was significantly lower compared to cefaclor monotherapy (Figure 2B). Following trimethoprim monotherapy at 0.25× its MIC, the stationary phase *B. thailandensis* population started to regrow after 9 h. Similarly, following combination therapy with 0.25× MIC trimethoprim and phage at an MOI of 1, the stationary phase *B. thailandensis* population started to regrow after 9 h and after 24 h reached a plateau that was significantly higher compared to that reached during phage monotherapy (red triangles and black circles in Figure 2C, respectively).

250 Taken together these data demonstrate that combination therapy with phage ΦBp-AMP1
251 increases the inhibitory efficacy of quinolones, β-lactams and tetracyclines, whilst combination
252 therapy with tetrahydrofolate synthesis inhibitors decreases the inhibitory efficacy of ΦBp-
253 AMP1.

254 **The interactions between phage ΦBp-AMP1 and antibiotics depend on the antibiotic**
255 **but not on the phage concentration**

256 Next, we set out to understand whether phage-antibiotic interactions in inhibiting bacterial
257 growth depend on either the antibiotic or the phage concentration. Firstly, we measured the
258 bacterial density of stationary phase *B. thailandensis* over time during exposure to LB medium
259 and different antibiotic concentrations at a constant phage MOI of 1 (data points in Figure 3A,
260 Figure 3F and Figure 3K). In order to estimate bacterial density and the associated uncertainty
261 also for antibiotic concentrations that we did not investigate experimentally, we fitted these
262 data to a statistical non-linear regression model (lines and bands in Figure 3A, Figure 3F and
263 Figure 3K). This model also allowed us to infer the probability of additivism between the phage
264 effect and the antibiotic effect on bacterial growth. We summarised our results in the form of
265 interaction plots [46] reporting bacterial density values in the absence of phage or antibiotic,
266 growth values following phage or antibiotic monotherapies and growth values following
267 combination therapy.

268 When ciprofloxacin was used above its MIC, we measured growth suppression following both
269 monotherapy and combination therapy (Figure 3A), without additive effect (blue shaded area
270 in Figure 3B and Figure 3E) in line with previous reports [46]. In contrast, when ciprofloxacin was
271 used at sub-inhibitory concentrations, the model predicted an interacting region: successful
272 growth suppression was achieved only in the case of combination therapy (red lines in Figure
273 3A), with a degree of confidence of >95% in predicted additive effect at ciprofloxacin
274 concentrations between 0.06 and 2 μg ml^{-1} (red shaded area in Figure 3B and Figure 3D).
275 This additive concentration range was broad for ciprofloxacin, finafloxacin and moxifloxacin
276 and narrower for nalidixic acid, ofloxacin and levofloxacin (Table S3). Finally, we did not record
277 an interaction effect between phage and ciprofloxacin at low concentrations (white shaded
278 area in Figure 3B and Figure 3C) in line with previous reports [46].

279 We recorded similar concentration-dependent interactions between phage and cefaclor
280 (Figure 3F-J); however, for this antibiotic the additive effect was limited to the antibiotic range
281 64-256 μg mL^{-1}, i.e. a 4-fold additive concentration range (Figure 3G). In addition, ceftazidime,
282 meropenem, doxycycline, tetracycline, amoxicillin and ampicillin displayed a narrow additive
283 concentration range (Table S3).

284

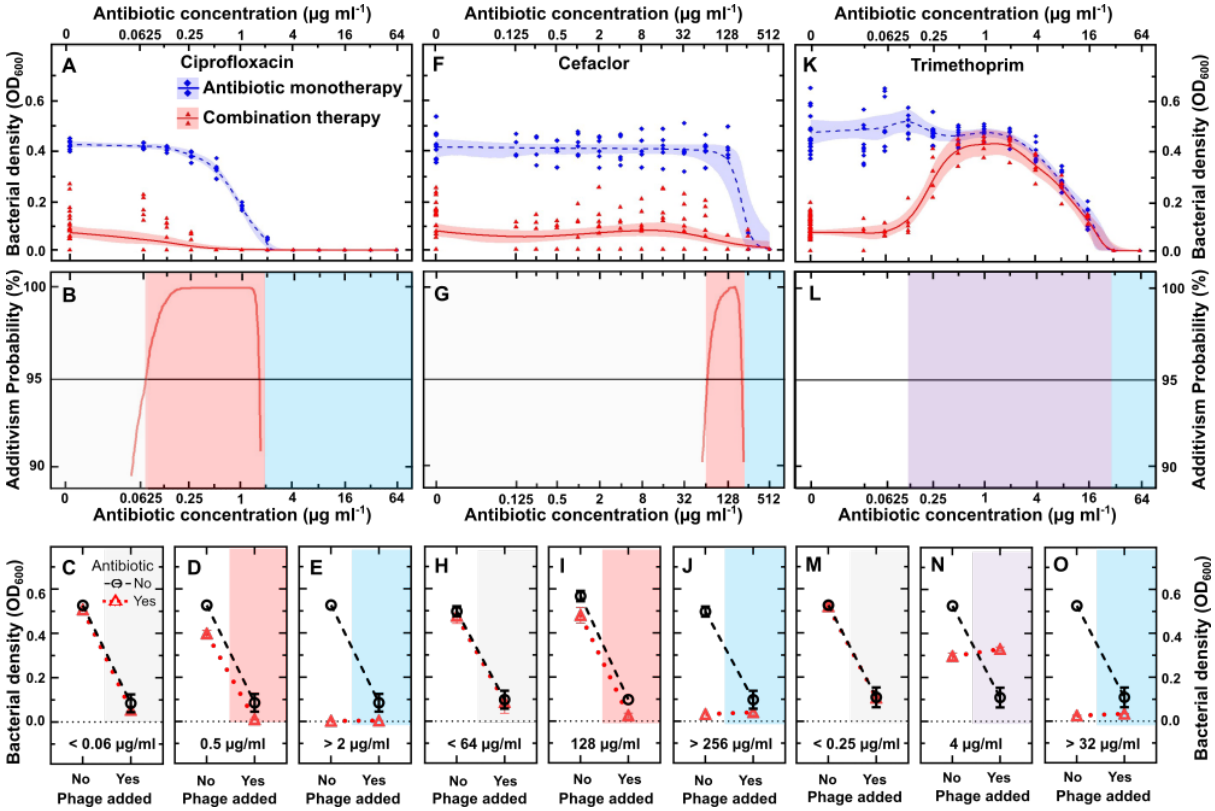

Figure 3 Interactions between ΦBp-AMP1 and antibiotics depend on the antibiotic concentration. Experimental data (symbols) and model predictions (lines and bands) describing the dependence of bacterial density on the concentration of (A) ciprofloxacin, (F) cefaclor or (K) trimethoprim in the absence (blue diamonds) and presence of phage ΦBp-AMP1 at an MOI of 1 (red triangles) after 24 h treatment. Each symbol represents the bacterial density measured in one of 15 technical replicates collated from biological triplicates. Some of the symbols overlap with each other. The lines and shaded areas are the medians, upper and lower quartiles, estimated by fitting our statistical non-linear regression model to our experimental data via Markov Chain Monte Carlo simulations. Corresponding predicted probability of an additive interaction between phage and (B) ciprofloxacin, (G) cefaclor and (L) trimethoprim (red lines) is shown only for antibiotic concentration ranges where the probability is higher than 90% (red shaded areas). Not shaded or blue shaded areas indicate antibiotic concentration ranges where the phage or the antibiotic dominate, respectively. Purple shaded areas indicate antagonism. Corresponding interaction plots at antibiotic concentrations selected from the ranges above for (C-E) ciprofloxacin, (H-J) cefaclor and (M-O) trimethoprim. Black circles connected by dashed lines show bacterial density values following control experiments and phage monotherapy, red triangles connected by dotted lines show bacterial density values following antibiotic monotherapy and combination therapy.

In contrast, we found an antagonistic effect when phage was used in combination with trimethoprim concentrations in the range of 0.125-32 μg mL^{-1} with the line connecting the growth value following antibiotic therapy and combination therapy (red, dotted line in Figure 3N) having a less negative slope than the line connecting the growth value following control experiments and phage monotherapy (black, dashed line in Figure 3N). A similarly extended antagonistic range was recorded when phage was used in combination with either sulfamethoxazole or co-trimoxazole.

Secondly, we measured the bacterial density of stationary phase *B. thailandensis* over time during incubation in LB medium while simultaneously varying the initial antibiotic concentration and phage MOI. We used ciprofloxacin, ampicillin and trimethoprim as representative molecules displaying a broad additive concentration range, a narrow additive concentration range and antagonism, respectively, in combination with phage at an initial MOI of either 10^{-4}, 10^{-2}, 10^{0} or 10^{2}. We found that growth inhibition was significantly extended below the MIC of ciprofloxacin or ampicillin even at a phage MOI of 10^{-4} (Figure 4A and Figure 4B), suggesting that a modest phage concentration is sufficient for increasing ciprofloxacin and ampicillin inhibitory efficacy against *B. thailandensis*.

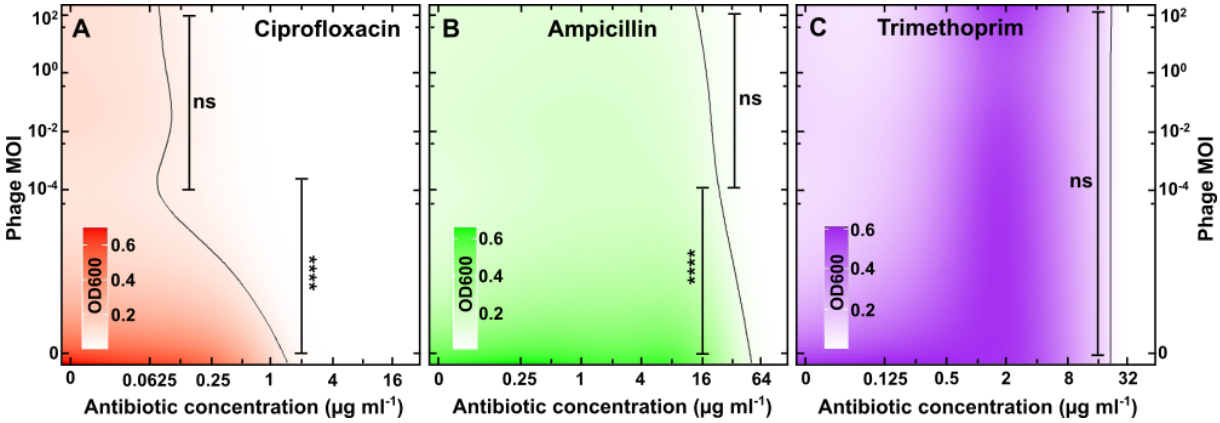

Figure 4 Phage-antibiotic interactions are not affected by the phage concentration. Heatmaps of *B. thailandensis* density (measured in OD_{600}) after 24 h treatment with different initial phage MOIs and different concentrations of (A) ciprofloxacin, (B) ampicillin or (C) trimethoprim. Heatmaps were obtained via hierarchical Bayesian statistical modelling fitted to our experimental data (measured only at the phage and antibiotic concentrations indicated on the x- and y-axes). The vertical black lines are predictions of all antibiotic-phage combinations that permit bacterial density values that are lower than 10% of the bacterial density values obtained for bacteria growing in LB medium only. ns indicates no statistical significance, **** indicates a p-value < 0.0001.

In contrast, growth inhibition was not extended below the MIC of trimethoprim at any of the phage MOIs tested (Figure 4C). Moreover, in the presence of phage *B. thailandensis* growth was maximal for trimethoprim concentrations in the range 1 – 8 μg mL^{-1} and decreased at lower trimethoprim concentrations (Figure 4C). Therefore, these data confirm the hypothesis above that sub-inhibitory concentrations of trimethoprim antagonize with phage efficacy to inhibit bacterial growth. Taken together, these data demonstrate that the interaction between phage ΦBp-AMP1 and antibiotics strongly depends on the antibiotic concentration and mode of action but not on the initial phage MOI.

Bactericidal effect of phage and ciprofloxacin combination therapy

We next set out to quantify the bactericidal efficacy of phage-antibiotic combination therapy. We exposed stationary phase *B. thailandensis* to a range of concentrations of ciprofloxacin

and phage at an MOI of 1 for 24 h, we quantified bactericidal efficacy by measuring survivors via CFU assays and calculated the survivor fold reduction compared to untreated bacteria (i.e. the higher the fold reduction in Figure 5A the stronger the bactericidal effect). Combined with phage, sub-MIC concentrations of ciprofloxacin allowed for a survivor fold reduction that was between 3 and 120 times greater compared to ciprofloxacin monotherapy (red and blue bars in Figure 5A, respectively); thus, suggesting a synergistic bactericidal effect between phage and ciprofloxacin, considering that phage monotherapy provided only a 2-fold survivor reduction (Figure 5A). Moreover, at supra-MIC concentrations, combination therapy achieved a survivor fold reduction that was between 570 and 2400 times greater compared to ciprofloxacin monotherapy. Notably, the minimum bactericidal concentration that provided complete eradication of stationary phase *B. thailandensis* (horizontal band in Figure 5A) was 8× MIC for ciprofloxacin monotherapy and 4× MIC for phage-ciprofloxacin combination therapy.

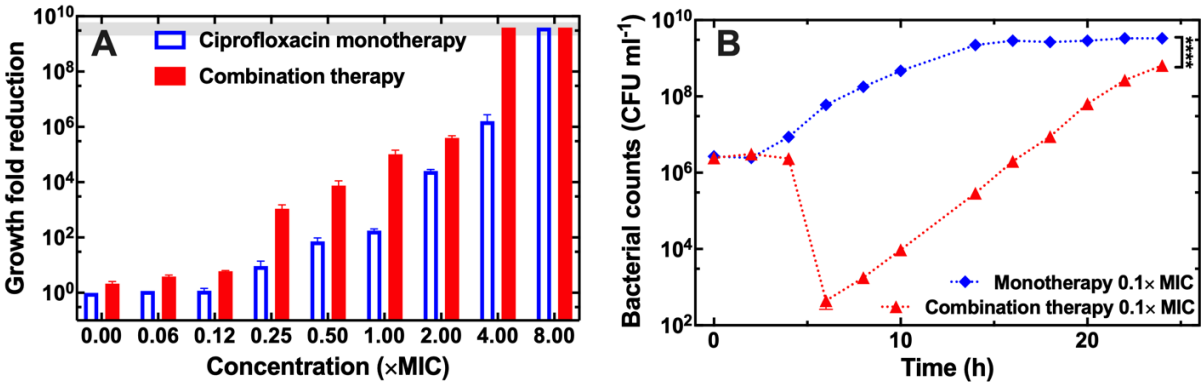

Figure 5 Synergistic bactericidal effect of phage and ciprofloxacin combination therapy. (A) Dependence of the ratio between the number of bacteria viable after 24 h incubation in LB medium and the number of bacteria viable 24 h ciprofloxacin monotherapy (blue bars) or phage-ciprofloxacin combination therapy (red bars) on the concentration of ciprofloxacin employed. In all cases the starting inoculum was stationary phase *B. thailandensis* at a concentration of 5×10^5 CFU mL^{-1} and bacteria were counted at 24 h via CFU assays. The grey horizontal band represents a survival fold reduction that corresponds to the complete eradication of the bacterial population, i.e. colony counts below limit of detection of 10 CFU mL^{-1}. (B) Temporal dependence of bacterial counts following 0.125× MIC ciprofloxacin monotherapy (blue diamonds) or combination therapy with 0.125× MIC ciprofloxacin and phage at an MOI of 1 (red triangles). Symbols and error bars are means and standard errors of the mean of biological triplicates each containing technical triplicates. Very small error bars cannot be visualised due to overlap with the datapoints. Dotted lines are guides-for-the-eye.

Next, we set out to measure and contrast the dynamics of the bactericidal effect of mono- and combination therapy at a sub-MIC antibiotic concentration. We treated stationary phase *B. thailandensis* with either ciprofloxacin at 0.125× its MIC or a combination of phage at an MOI of 1 and ciprofloxacin at 0.125× its MIC and measured the number of survivors at regular time points via CFU assays (Figure 5B). Following ciprofloxacin monotherapy the bacterial population was not affected by antibiotic exposure but started expanding after 2h of treatment and reached stationary phase after 14h of treatment (blue diamonds in Figure 5B). In contrast, following combination therapy the bacterial population reduced between 4 h and 6 h and

375 reached a minimum that was >5-log lower compared to the initial bacterial inoculum (red
376 triangles in Figure 5B). The surviving bacterial population started to increase after 6 h of
377 treatment due to the emergence of phage resistance (Figure S5) and reached a maximum
378 level at 24 h that was 1-log lower than bacteria treated with ciprofloxacin monotherapy (red
379 triangles and blue diamonds in Figure 5B, respectively). Taken together these data confirm
380 that the use of ΦBp-AMP1 allows a reduction in the concentration of antibiotic required to both
381 inhibit growth of or kill stationary phase *B. thailandensis*.

382

383 **Synergistic bactericidal interactions between phage and antibiotics are underpinned**
384 **by phage-induced downregulation of efflux in *B. thailandensis***

385 Next, we set out to discover the molecular mechanisms underpinning the newly found
386 synergistic bactericidal interaction between ΦBp-AMP1 and ciprofloxacin. We treated
387 stationary phase *B. thailandensis* for 4 h either with 0.125× MIC ciprofloxacin monotherapy or
388 phage monotherapy at an MOI of 1 or combination therapy with both 0.125× MIC ciprofloxacin
389 and phage at an MOI of 1. We chose 4 h-long treatments because these treatments returned
390 similar survivor numbers before the > 5-log reduction in survivor numbers measured for
391 combination therapy at the 6 h time point (Figure 5B). We extracted bacterial and phage RNA
392 from biological triplicates of each condition and performed a global comparative transcriptomic
393 analysis [54] among the transcriptomes obtained from these three different conditions and with
394 respect to stationary phase *B. thailandensis* incubated in LB medium for 4 h (Supplementary
395 files 1-3). Using principal component analysis, we found that bacterial transcriptome replicates
396 from each condition clustered together and were well separated from replicates from different
397 conditions (Figure S6A). The only exception were the bacterial transcriptomes harvested from
398 cultures treated with phage mono- and combination therapy (black circles and red triangles in
399 Figure S6A) that largely overlapped, suggesting that, at the concentrations employed, phage
400 had a greater impact than ciprofloxacin on the bacterial transcriptomes. Moreover, the phage
401 transcriptomes harvested from cultures treated with mono- and combination therapies also
402 largely overlapped according to our principal component analysis (Figure S6B).

403 Gene ontology enrichment analysis [55] of differentially expressed genes revealed that all
404 treatments investigated resulted in the downregulation of locomotion processes, in
405 accordance with a recent study using *P. aeruginosa* [56], as well as cell localization, cell
406 projection, organelle organization and response to external stimuli processes (Figure 6A, 6B
407 and Supplementary files 4-6). Ciprofloxacin monotherapy also caused the downregulation of
408 biological processes involved in cell communication, as well as the upregulation of RNA,
409 catabolic, metabolic and ribosomal processes (Figure 6A and Supplementary file 4).

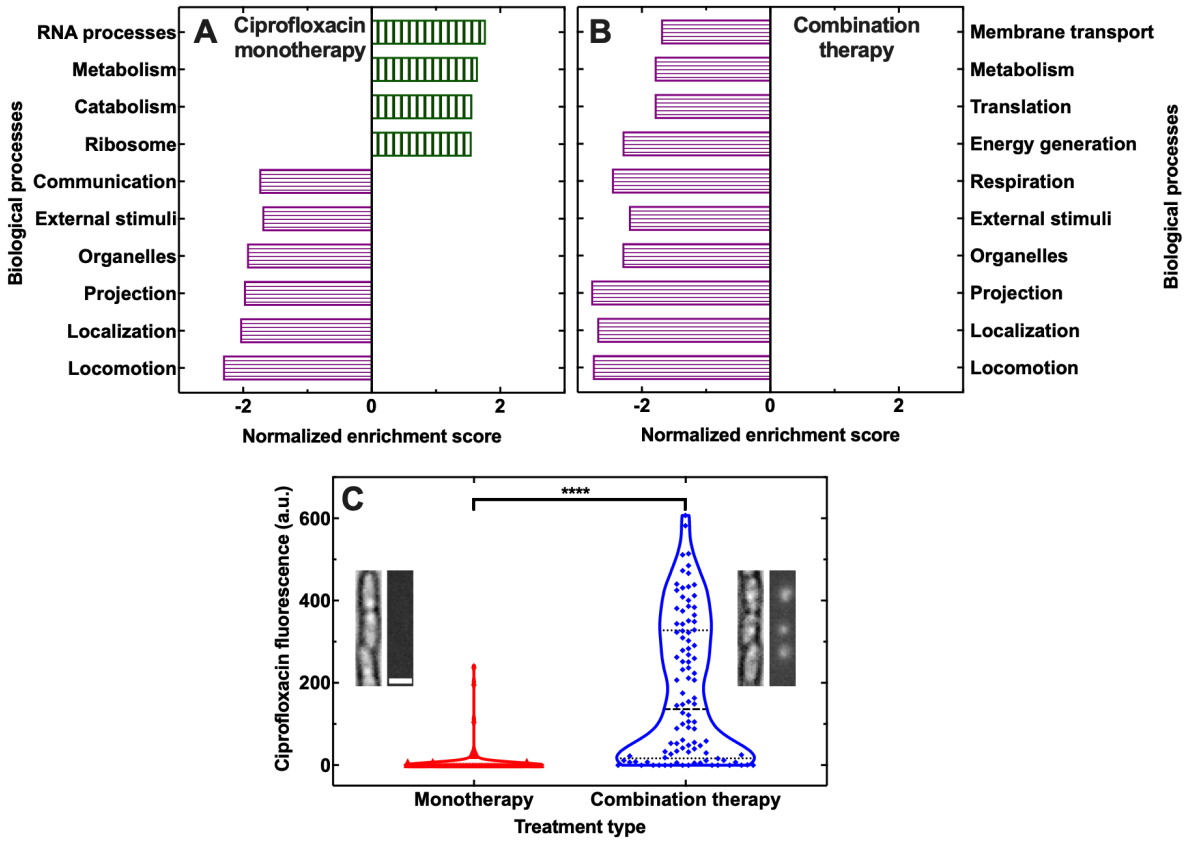

Figure 6 Synergistic bactericidal interactions between phage and ciprofloxacin are underpinned by phage-induced downregulation of membrane transport in *B. thailandensis*. Major biological processes that are significantly enriched and either up- or downregulated (vertically and horizontally patterned bars, respectively) in stationary phase *B. thailandensis* after 4 h of (A) monotherapy with ciprofloxacin at 0.125× MIC or (B) combination therapy with ciprofloxacin at 0.125× MIC and phage at an MOI of 1 with respect to untreated *B. thailandensis* incubated for 4 h in LB medium only. Corresponding differential gene expression analyses and gene ontology enrichment analyses are reported in Supplementary files 1-3 and 4-6, respectively. (C) Distribution of values of fluorescence of ciprofloxacin-NBD accumulating in N = 100 individual stationary phase *B. thailandensis* that had been incubated for 4 h in either ciprofloxacin-NBD only or ciprofloxacin-NBD and phage (red triangles and blue diamonds, respectively). Ciprofloxacin-NBD was introduced in the microfluidic device at t = 0 at a concentration of 32 µg ml^{-1}, phage was introduced at t = 0 at a concentration of 10^8 PFU ml^{-1}. Dashed lines indicate the median of each distribution, dotted lines indicate the quartiles of each distribution. **** indicate a p-value < 0.0001.

In contrast, both phage monotherapy and combination therapy caused the downregulation of metabolic, membrane transport, translational, energy generation and respiration processes (Figure 6B and Supplementary files 5 and 6). Specifically, genes encoding the major efflux pump BpeEF-OprC were significantly downregulated along with functional subunits of the F_0F_1-type ATP synthases, of the cytochrome O oxidase, of the NADH-quinone oxidoreductase complex, of lipopolysaccharide transport and of secretion systems (Supplementary file 2).

Combination therapy drove a global differential gene regulation that was very similar to that caused by phage monotherapy and gene ontology enrichment analysis did not return any enriched functional category for this comparison. Moreover, the expression of phage encoded

genes was also unaffected by the presence of ciprofloxacin (Supplementary file 7) and gene ontology enrichment analysis did not return any enriched functional category for this comparison either.

Next, we set out to test the hypothesis that phage-induced downregulation of efflux processes led to increased intracellular accumulation of ciprofloxacin during phage-ciprofloxacin combination therapy. We used our recently reported microfluidics-based time-lapse microscopy platform [57,58] and a fluorescent derivative of ciprofloxacin (i.e. ciprofloxacin-nitrobenzoxadiazole, henceforth ciprofloxacin-NBD) to measure intracellular accumulation of ciprofloxacin in individual stationary phase *B. thailandensis* cells. In accordance with our hypothesis, we found that the distribution of ciprofloxacin-NBD fluorescence values after 4 h phage-ciprofloxacin-NBD combination therapy was significantly higher than the distribution of ciprofloxacin-NBD fluorescence values after 4 h ciprofloxacin-NBD monotherapy (Figure 6C).

Moreover, using this platform we did not find evidence of either cell filamentation or a significant difference in cell size between stationary phase *B. thailandensis* incubated in LB growth medium only (Figure S7 A-E), or during phage monotherapy (Figure S7 F-J) or during combination therapy with phage at an MOI of 1 and ciprofloxacin at 0.125× MIC (Figure S7 K-O). We found that stationary phase *B. thailandensis* infected with phage in the presence of sub-inhibitory concentrations of ampicillin or ciprofloxacin produced less phage particles than in the absence of antibiotics in planktonic cultures and plaques of similar size on agar cultures (Figure S1 and S8, respectively). Sub-inhibitory concentrations of trimethoprim also led to smaller plaques with phage propagation starting significantly later in the presence of trimethoprim (Figure S1 and S8). We also did not observe plaque formation on LB agar plates in the presence of sub-inhibitory concentrations of ciprofloxacin in the absence of phage ΦBp-AMP1. Moreover, in our phage transcriptome analysis we found evidence of expression of structural phage proteins, but we did not find evidence of expression of genes encoding excisionases, i.e. proteins required for the excision of dormant phage from within the hosts genome [59], neither during phage mono- nor combination therapy (Supplementary file 7). However, it is conceivable that one or more of the 11 hypothetical proteins expressed by ΦBp-AMP1 (Supplementary file 7) could perform excisionase activity.

Taken together these data demonstrate that the observed phage-antibiotic interactions are not due to cell filamentation, increase phage particle production or phage induction in the presence of antibiotics but are instead underpinned by phage-induced downregulation of membrane transport and energetic processes that are involved in the efflux of ciprofloxacin leading to higher intracellular ciprofloxacin accumulation in the presence of phage.

473 **Discussion**

Emergence of resistance to phage

474 Phage and bacteria are engaged in a constant arms race leading to the evolution of a multitude
475 of non-mutually exclusive antiphage defence mechanisms, including the well-understood
476 phage receptor alteration, restriction-modification, abortive infection, CRISPR-Cas systems,
477 as well as new defence systems whose mechanisms are still unknown [60,61]. It is well
478 established that increased phage virulence selects for the evolution of host resistance if the
479 costs associated with resistance are outweighed by the benefits of the capability to avoid
480 infection [62,63]. Accordingly, we found that the level of resistance to phage increased with the
481 strength of phage predation. Interestingly, even within a putatively clonal *B. thailandensis*
482 population we found evidence of emergence of different levels of resistance due to mutations
483 in eight different genes. Three of these genes encoded glycosyltransferase and O-antigen
484 synthesis, that are strongly linked with the LPS [64,65], and capsular polysaccharides. Our data
485 therefore suggest that the LPS or capsular polysaccharides could be the receptors for phage
486 ΦBp-AMP1. This hypothesis is further corroborated by our global comparative transcriptomics
487 analysis demonstrating the downregulation of LPS assembly associated genes following
488 exposure to ΦBp-AMP1. Indeed, the LPS is a well-known receptor for many different
489 bacteriophages [66–68] and mutations of LPS confer resistance to phage in a variety of bacteria
490 [69] [70], whereas capsular polysaccharides have recently been shown to serve as primary
491 receptors of *E. coli* phage [71] [72]. Moreover, it has been reported that *B. pseudomallei* displays
492 various colony morphotypes based on O-antigen variations [73] [74]. Accordingly, we have
493 demonstrated that phage-resistant bacteria form smaller colonies compared with the parental
494 strain while displaying mutations in genes associated with O-antigen synthesis.

495 **Phage-antibiotic interactions**

496 The interactions between two or more antimicrobials as components of combination therapies
497 are broadly classified in three main types: additive (the sum of the effect of each component),
498 synergistic (a larger-than-additive effect) and antagonistic (a smaller-than-additive effect [76–
499 79]). In the context of phage-antibiotic therapy instead, phage-antibiotic synergy has been
500 defined as the stimulation of phage replication when bacteria are treated with sub-inhibitory
501 concentrations of antibiotics [7,9,37]. Considering that in accordance with a recent report [75] we
502 did not find stimulation of phage replication in the presence of antibiotics, we chose to use the
503 more broadly accepted definitions of additive, synergistic and antagonistic interactions,
504 introduced above [76,77]. Specifically, by using statistical analysis on interaction plots we found
505 an additive effect between the phage and most of the tested molecules from the quinolone, β-
506 lactam and tetracycline antibiotic classes, antagonism between the phage and

507 tetrahydrofolate synthesis inhibitors and bactericidal synergy between the phage and the
508 quinolone ciprofloxacin. These effects were comparable or more efficient in suppressing
509 bacterial growth than previously reported synergistic phage-antibiotic effects [37,45,46]. For
510 example, ceftazidime efficacy increased by a factor of 2 compared to ceftazidime monotherapy
511 when used in combination with the podovirus vB_BpP_HN01 [80] or the myovirus KS12 [9] against
512 *B. pseudomallei* or *B. cenocepacia*, respectively; we measured an 8-fold increase in
513 ceftazidime efficacy against *B. thailandensis* in the presence of phage ΦBp-AMP1. Using the
514 temperate phage HK97 in combination with ciprofloxacin, a previous study has reported
515 bactericidal synergy against *E. coli* K12, with complete eradication being achieved at 0.5× MIC
516 ciprofloxacin [42]; we measured a comparatively weaker bactericidal synergy between ΦBp-
517 AMP1 and ciprofloxacin, with complete eradication being achieved at 4× MIC ciprofloxacin.
518 However, it is worth noting that stationary phase *B. thailandensis* is significantly more resistant
519 than exponential phase *E. coli* K12 with ciprofloxacin MIC values of 2 and 0.2 μg/ml,
520 respectively.

521 **Factors affecting phage-antibiotic interactions**

522 The dependence of phage-antibiotic interactions on the antibiotic class is well established
523 [7,9,37,46,75,81], although the mechanisms underpinning this dependence remain largely unknown
524 [31]. For example, the myovirus KS12 broadly synergised with quinolones, β-lactams and
525 tetracycline when used to inhibit growth of *B. cenocepacia* but antagonised with
526 aminoglycosides [9]. The myovirus ΦHP3 displayed a synergistic effect with ceftazidime, an
527 additive effect with kanamycin and an antagonistic effect with chloramphenicol when used to
528 inhibit growth of *E. coli* [46]. The phage PYO^{SA} antagonised tetracycline, azithromycin, and
529 linezolid but synergised with daptomycin, vancomycin and kanamycin when used to inhibit
530 growth of *S. aureus* [45]. Here we advance this understanding by showing that even molecules
531 within the same class can display a dramatically different extent and range of additive
532 interactions with the same phage and that when used with phage the same molecule can
533 simultaneously display an additive effect in inhibiting bacterial growth and a synergistic effect
534 in killing bacteria.

535 The outcome of phage-antibiotic therapy is often contradictory because of a lack of systematic
536 analysis of interactions between phage and antibiotics: these interactions are often studied
537 with only one or two concentrations of the antimicrobials, which are wholly insufficient in
538 predicting combinatorial concentrations that are effective during treatment [28,46]. By assessing
539 bacterial growth when exposed to multiple orders of magnitude of antibiotic concentrations
540 and phage titers, we discovered that phage-antibiotic interactions strongly depend on the
541 antibiotic concentration employed, but surprisingly do not vary with phage titer, a difference

542 from previous findings [46]. These newly discovered dependences should be taken into account
543 when designing rational phage-antibiotic therapy [28,29]. In fact, our data suggest that it might be
544 relatively straightforward to hit a suitable ΦBp-AMP1 phage titer in an *in vivo* setting, where
545 phage are broadly tolerated [82] but their pharmacokinetic and pharmacodynamic parameters
546 are less known compared to antibiotics [83].

547 **Mechanistic understanding of antibiotic-phage interactions**

548 The additive effects between phage and antibiotics are stronger and broader in our
549 experiments compared to previous reports [7,9], [80], possibly due to differences at the phage
550 level, i.e., a podovirus vs a myovirus, at the bacterial strain and physiology level, i.e., stationary
551 phase *B. thailandensis* vs exponential phase *B. cenocepacia*, or due to a different mechanism
552 of interaction between phage and antibiotics. Indeed, KS12 and a variety of other phage
553 displayed an increase in plaque size and phage titer in the presence of sub-inhibitory
554 concentrations of antibiotics [7,34,37,41], possibly caused by the acceleration of phage assembly
555 and cell lysis due to cell filamentation in the presence of antibiotics [9,37,46,84]. In contrast, we did
556 not find evidence neither of cell filamentation nor of an increase in plaque size and phage titer
557 in the presence of sub-inhibitory concentrations of quinolones, β-lactams or tetracyclines.
558 Reduced phage titer in the presence of sub-inhibitory concentrations of trimethoprim could
559 instead explain the observed antagonism between ΦBp-AMP1 and trimethoprim. Moreover,
560 temperate phage activity is known to enhance antibiotic efficacy through depletion of lysogens
561 [42]. Although we found evidence of prophage ΦE125 and ΦE12-2 [85,86], it is unlikely that
562 depletion of ΦE125 or ΦE12-2 lysogens plays a role in our experiments since we did not find
563 evidence of plaque formation in the presence of ciprofloxacin, that is a lysogen activating
564 antibiotic [42], in the absence of ΦBp-AMP1.

565 Based on our global gene expression analysis, we hypothesized that antibiotics are more
566 effective in inhibiting *B. thailandensis* growth in the presence of ΦBp-AMP1 due to phage-
567 induced down-regulation of antibiotic efflux out of the cell. Indeed, the multi-drug efflux pump
568 BpeEF-OprC [87] was downregulated in the presence of phage and it is known that deletion of
569 BpeEF-OprC causes increased susceptibility to quinolones and β-lactams [88]. Moreover, we
570 detected a strong downregulation of genes associated with aerobic respiration and
571 transmembrane transport of protons, effectively reducing the availability of ATP for active
572 transport of substrates as well as the proton motive force. A reduction in proton motive force
573 levels leads to reduced antibiotic efflux [90–92], and in the long-term selection for mutations in
574 drug efflux components [93]. In accordance with our hypothesis, we found that a fluorescent
575 derivative of ciprofloxacin accumulates in individual *B. thailandensis* cells at significantly
576 higher levels in the presence of ΦBp-AMP1 compared with in its absence. Noteworthy,

577 previous studies using phage that have the efflux component TolC as a receptor,
578 demonstrated that emergence of phage resistance in bacteria via *tolC* mutations led to
579 increased antibiotic susceptibility [70,94,95]. Finally, it is conceivable that the phage-antibiotic
580 interactions we observed are also due to phage and antibiotics targeting cells in different
581 metabolic states as recently hypothesised [75].

582 In summary, the interactions between phage and bacteria are multifaceted and complex due
583 to a billion-year long arms race between both entities [96–100] and are further modified when a
584 second selective pressure is imposed, such as the presence of antibiotic compounds secreted
585 by other microbes in the environment [97,101]. Understanding such interactions might hold the
586 key for successful antimicrobial therapy and to overcome the current antimicrobial resistance
587 crisis [1]. Considering that stationary phase bacteria are traditionally refractory to antibiotics,
588 especially in spatial structures such as biofilms where antibiotic diffusion is further hindered
589 [52], our data offer a potential route for their eradication by combining low doses of clinically
590 relevant antibiotics with low doses of phage, that should be easily obtainable *in vivo* thanks to
591 the self-propagating nature of phage.

592 **Materials and Methods:**

593 **Key Resources Table**

REAGENT or RESOURCE	Source	Identifier
Bacterial and phage strains		
B. thailandensis E264	(Kim et al., 2005)	RefSeq: NC_007650/51
ΦBp-AMP1	(Gatedee et al., 2011)	RefSeq: NC_047743
Chemicals		
Amoxicillin	Sigma-Aldrich	Cat# A8523
Ampicillin	Sigma-Aldrich	Cat# A9518
Cefaclor	Sigma-Aldrich	Cat# C6895
Ceftazidime	Melford	Cat# C59200
Ciprofloxacin	Sigma-Aldrich	Cat# 17850
Doxycycline	Sigma-Aldrich	Cat# D9891
Finafloxacin	Sigma-Aldrich	Cat# SML2134
Levofloxacin	Sigma-Aldrich	Cat# 40922
Linezolid	Sigma-Aldrich	Cat# O9409
Meropenem	Sigma-Aldrich	Cat# M2574
Moxifloxacin	Sigma-Aldrich	Cat# PHR1542
Nalidixic acid	Sigma-Aldrich	Cat# N8878
Ofloxacin	Sigma-Aldrich	Cat# O8757
Roxithromycin	Sigma-Aldrich	Cat# R4393
Sulfamethoxazole	Sigma-Aldrich	Cat# S7507
Tetracycline	Sigma-Aldrich	Cat# 87128
Trimethoprim	Sigma-Aldrich	Cat# T7883
Vancomycin	Sigma-Aldrich	Cat# 94747
Software and algorithms		
R version 3.4.1	(R Core Team, 2017)	https://cran.r-project.org
brms R package	(Bürkner, 2017)	https://cran.r-project.org
breseq	(Deathrage and Barrick,	https://barrickslab.org
ImageJ	(Schneider et al., 2012)	https://imagej.nih.gov
GraphPad Prism 8.3.0	GraphPad	https://www.graphpad.com/
PHASTER	University of Alberta, Canada	https://phaster.ca
Other		
CLARIOstar plate reader	BMG Labtech	
WPA cell density meter	Scientific Laboratory Supplies	Cat# CO8000
Sartorius Minisart™ 0.2 µm	Fisher Scientific	Cat# 10730792
RNeasy Mini Kit (50)	QIAGEN	Cat# 74104
Qubit 1.0 Fluorometer	Invitrogen	Cat# Q32857
IX73	Olympus, Tokyo, Japan	
UPLSAPO60XW	Olympus, Tokyo, Japan	
Flow Unit S	Fluigent	
MFCS-4C	Fluigent	
Zyla 4.2	Andor	

594

595

596 **Bacterial and bacteriophage strains**

597 *B. thailandensis* E264 strain and the temperature dependent, lytic bacteriophage ΦBp-AMP1
598 [48] were obtained from the Department of Immunology, Faculty of Medicine Siriraj Hospital,
599 Mahidol University.

600 **Bacterial culturing**

601 *B. thailandensis* was stored at -80 °C and streaked on Lysogeny broth (LB, 10 g/L Tryptone,
602 5 g/L Yeast extract, 10 g/L NaCl, Melford) agar plates (10 g/L, 1.5% Agar) every two weeks.
603 Overnight cultures were setup by inoculating a single *B. thailandensis* colony from a plate into
604 flasks containing 50 mL of LB broth and were grown for 17 h at 37 °C on shaking platforms
605 set at 200 rpm.

606 **Propagation and titration of phage**

607 Phage propagation was carried out as previously reported [51]. Briefly, overnight cultures of *B.*
608 *thailandensis* E264 were diluted 1000× in 50 mL LB medium to obtain a bacterial concentration
609 of approximately 2×10^6 CFU mL^{-1}. These sub-cultures were then incubated for 4 h at 37 °C
610 and 200 rpm, allowing them to reach early exponential phase (~8×10^6 CFU mL^{-1}). Then, these
611 sub-cultures were infected with ΦBp-AMP1 at an MOI = 0.01 and incubated for 17 h at 37 °C
612 and 200 rpm. On the following day, cells were pelleted by centrifugation for 40 minutes at 3000
613 *g* and the phage-containing supernatant was filtered twice (Sartorius Minisart™ 0.2 µm) to
614 obtain a phage stock. The phage concentration within this stock was then determined via the
615 double agar overlay technique [102]. Briefly, LB top agar (10 g/L, 0.5% Agar) was melted in a
616 microwave and allowed to cool to below 40 °C. An aliquot of an overnight *B. thailandensis*
617 E264 culture was added to the melted top agar at a volume: volume concentration of 1:50. LB
618 agar plates were subsequently coated in a thin layer of the top agar above creating a
619 continuous bacterial lawn. In parallel, a 10-fold dilution series of the phage stock was prepared
620 in LB medium. Phage was then titred using the standard double agar overlay technique [103].
621 All plates were then incubated at 37 °C for 17 h after which the phage induced plaques in the
622 bacterial lawn were counted and the plaque forming units (PFU) per mL^{-1} of the phage stock
623 was calculated. Phage stocks were stored at 4 °C for a maximum of two weeks before a new
624 propagation was performed. Prior to each use, the phage concentration within the phage stock
625 was determined via the double agar overlay technique above.

626 **Bacterial growth in the presence of phage**

627 In order to measure the growth of bacteria in the presence of phage we used two independent
628 approaches. Firstly, we measured the concentration of bacteria during phage infection over

629 time using colony forming unit (CFU) assays [54]. Briefly, three overnight cultures of *B.*
630 *thailandensis* were diluted in 50 mL LB medium to obtain a bacterial concentration of
631 approximately 2×10^6 CFU mL^{-1}. ΦBp-AMP1 was added to these three sub-cultures at an MOI
632 of 1 and the sub-cultures were incubated at 37 °C and 200 rpm. Triplicate aliquots were taken
633 from each infected sub-culture every two hours, serially diluted in LB and plated on LB agar
634 plates. These plates were incubated 37 °C for 24h before counting CFU on each plate to
635 calculate the bacterial concentration at each time point in each sub-culture as the mean and
636 standard error of the mean of biological triplicate each containing technical triplicate. The
637 growth of control uninfected cultures was measured in a similar manner without the addition
638 of phage. Secondly, we measured the change of bacterial density over time during phage
639 infection by measuring the optical density of growing sub-cultures. Briefly, three overnight
640 cultures of *B. thailandensis* were diluted in LB in the wells of a 96 well plate and mixed with
641 phage to obtain a final bacterial concentration of 5×10^5 CFU mL^{-1} and a final phage MOI of
642 either 10^{-4}, 10^{-2}, 1 or 10^2. The plates were the incubated at 37 °C and 200 rpm and the optical
643 density of each well was measured every 10 min via a CLARIOstar plate reader system (BMG)
644 and blank corrected to the optical density measured in wells containing LB medium only. Each
645 condition was tested in 84 technical replicates obtained from biological triplicate.

646 **Determination of heritable resistance to phage**

647 In order to determine whether heritable resistance to phage had emerged in bacteria from
648 wells where we measured bacterial growth in the presence of phage, we re-inoculated these
649 survivors in wells of a 96-well plate containing LB and phage at a concentration of ~5×10^5
650 PFU mL^{-1}. We incubated these plates at 37 °C and 200 rpm for 24 h and measured the optical
651 density as described above. We employed this same approach to determine whether heritable
652 resistance to phage had emerged in bacteria from wells where we measured bacterial growth
653 in the presence of both phage and each of the antibiotics reported in Table 1.

654 **Determination of colony size**

655 To determine whether phage-resistance comes at a fitness cost in colony size we performed
656 image analysis experiments of bacteria from wells where we measured bacterial growth in the
657 presence of phage. These survivors were plated onto LB agar plates alongside uninfected
658 bacteria from separate control experiments. The plates were then incubated at 37 °C for 72 h
659 and were imaged with a Xiaomi Mi A2 mobile phone camera at 24 h intervals. The colony size
660 was determined via image analysis of 150 colonies for each condition and time point using the
661 ImageJ software.

662

663 **Phage growth in the presence of antibiotics**

664 Overnight cultures of *B. thailandensis* E264 were diluted 1000× in 50 mL LB medium to obtain
665 a bacterial concentration of approximately 2×10^6 CFU mL^{-1}. ΦBp-AMP1 was added to these
666 sub-cultures at an MOI of 1 and the sub-cultures were incubated at 37 °C and 200 rpm. In
667 separate experiments, ΦBp-AMP1 was added at an MOI of 1 together with either ampicillin or
668 ciprofloxacin or trimethoprim at 0.25× their respective MIC. 1 mL triplicate aliquots were taken
669 from the infected sub-cultures at two-hour intervals for twenty-four hours and the phage
670 propagation over time was monitored by determining plaque forming units per millilitre via the
671 double agar overlay technique above. Each experiment was then performed in biological
672 triplicate.

673 **Determination of antibiotic minimum inhibitory concentrations and the impact of phage**
674 **on antibiotic efficacy**

675 The minimum inhibitory concentration (MIC) of each antibiotic employed was determined via
676 the broth dilution method [104]. Briefly, each antibiotic was dissolved according to the
677 manufacture's specifications and diluted in a two-fold dilution series in LB medium within wells
678 of a 96-well plate. Stationary *B. thailandensis* E264 bacteria were then added at a final
679 concentration of 5×10^5 CFU mL^{-1} to each well. The plates were incubated at 37 °C and 200
680 rpm and after 24 h the optical density of each well was measured via a CLARIOstar plate
681 reader system (BMG) and blank corrected to the optical density measured in wells containing
682 LB medium only. The minimum inhibitory concentration was determined as the minimum
683 concentration of antibiotic for which we measured an optical density value that was less than
684 10% of the optical density value that we measured in wells containing LB medium and bacteria
685 only. All MIC assays were performed at least in biological and technical triplicate from which
686 mean and standard error of the mean were calculated. Next, to determine the influence of
687 ΦBp-AMP1 on the efficacy of each antibiotic, the experiments above were repeated with the
688 addition of ΦBp-AMP1 at an MOI of 1 (i.e. 5×10^5 PFU mL^{-1}).

689 **Determination of time-dependent bacterial growth in the presence of antibiotic and**
690 **phage**

691 Overnight cultures of *B. thailandensis* E264 were diluted to a concentration of ~5×10^5 CFU
692 mL^{-1} in LB medium in wells of a 96-well plate, together with either ΦBp-AMP1 at an MOI of 1,
693 or levofloxacin, cefaclor or trimethoprim at 0.25× their respective MIC, or both ΦBp-AMP1 at
694 an MOI of 1 and either levofloxacin, cefaclor or trimethoprim at 0.25× their respective MIC.
695 Each plate were then incubated for 24 h in a CLARIOstar plate reader (BMG) at 37 °C and
696 200 rpm, measuring optical density at λ=600nm (OD_{600}) every 30 min. Each experiment was

697 repeated in biological and technical triplicate from which we calculated mean and standard
698 error of the mean of each measurement.

699 **Bacterial killing assays**

700 Bacterial killing assays were performed as previously reported [54]. Briefly, overnight cultures of
701 *B. thailandensis* E264 were diluted 1000× in 50 mL fresh LB growth medium and infected with
702 either solely ciprofloxacin (at a concentration between 0.625× and 8× the MIC), or a
703 combination of ciprofloxacin and phage at MOI = 1. The cultures were incubated at 37 °C and
704 200 rpm for 24 h after which the colony count (CFU mL^{-1}) was determined as reported above.
705 We quantified bactericidal efficacy of each treatment as the ratio of the colony counts in
706 untreated control experiments over the colony counts measured in each treatment.

707 **Determination of heritable resistance to antibiotics**

708 In order to determine whether heritable resistance to antibiotics had emerged in bacteria from
709 wells where we measured bacterial growth in the presence of phage and antibiotics, we re-
710 inoculated these survivors in wells of a 96-well plate containing LB and either phage at a
711 concentration of ~5×10^5 PFU mL^{-1}, or the antibiotic employed at a concentration in range
712 0.125-128 µg ml^{-1}, or both phage at a concentration of ~5×10^5 PFU mL^{-1} and the antibiotic
713 employed at a concentration in range 0.125-128 µg ml^{-1}. We incubated these plates at 37 °C
714 and 200 rpm for 24 h and measured the optical density as described above.

715 **Determination of the impact of antibiotics on plaque size**

716 To determine whether phage plaque sizes may be influenced by the presence of antibiotics,
717 we implemented a previously reported protocol [37]. Briefly, LB top agar was melted in a
718 microwave and allowed to cool below 40 °C. An aliquot of an overnight *B. thailandensis* E264
719 culture was added to the melted top agar at a volume: volume concentration of 1:50 alongside
720 phage at a concentration of 10^1 PFU mL^{-1} and either ciprofloxacin, trimethoprim or ampicillin
721 at 0.5× and 0.125× of their respective monotherapy MICs. The resulting mixture was added to
722 the top agar. The top agar was then well mixed by inversion, plated evenly onto LB agar plates
723 (10 g/L, 1.5% Agar) and incubated for 24 h at 37 °C. The plates were then imaged using a
724 Xiaomi Mi A2 mobile phone camera. The plaque size was determined via image analysis of
725 120 plaques for each condition in biological triplicate using the ImageJ software.

726 **Determination single-cell morphology and ciprofloxacin accumulation**

727 To measure the size and morphology of individual bacterial during phage-monotherapy or
728 antibiotic-phage combination therapy, we deployed the microfluidic mother machine device as
729 previously described [105]. Briefly, the device consists of a central channel that measures 25

730 and 100 μm in height and width, respectively, and six thousand lateral side channels, each 1
731 μm in width and height and 25 μm in length [106]. Bacteria were prepared by pelleting an
732 overnight culture of *B. thailandensis* for 15 minutes at 3000 *g*. The resulting bacterial pellet
733 was resuspended at a previously optimised nominal OD_{600} of 50 [106], in medium obtained by
734 double filtering the supernatant from the spun down culture using 0.22 μm filters. These
735 bacteria were then introduced in the central channel of the mother machine device from where
736 they reached the lateral channel at an average concentration of one bacterium per channel
737 [107]. Next, the device was mounted on an inverted microscope (IX73 Olympus, Tokyo, Japan)
738 located in a temperature-controlled chamber kept at 37 °C. Fluorinated ethylene propylene
739 tubing (1/32" × 0.008") was connected to the device as inlet and outlet tubes further connected
740 to a computerised pressure-based flow control system (MFCS-4C, Fluigent) [108]. Next, LB
741 medium only or LB medium containing 2×10^8 PFU mL^{-1} phage or LB medium containing 2×10^8
742 PFU mL^{-1} phage and 0.125× MIC ciprofloxacin was continuously supplied in the device at a
743 constant flow rate of 100 μl/h. Simultaneously, bright field images of 20 areas of the mother
744 machine, each containing 23 lateral channels were acquired at 2 min intervals via a 60× 1.2
745 N.A. objective (UPLSAPO60XW, Olympus) and an sCMOS camera with an exposure time of
746 0.01 s (Zyla 4.2, Andor, Belfast, United Kingdom) controlled via Labview [109,110]. This
747 microfluidics-microscopy platform was also used to quantify the accumulation of ciprofloxacin
748 as previously reported [52,111,112]. Briefly, LB medium containing a fluorescent ciprofloxacin
749 derivative, i.e. ciprofloxacin-nitrobenzoxadiazole (ciprofloxacin-NBD) or ciprofloxacin-NDB
750 and 2×10^8 PFU mL^{-1} phage was continuously supplied in the device at a constant flow rate of
751 100 μl/h. In both cases ciprofloxacin-NBD was supplied at a concentration of 32 μg ml^{-1}. Bright
752 field images were acquired as described above together with corresponding fluorescence
753 images acquired by exposing the bacteria for 0.03 s to the blue excitation band of a broad-
754 spectrum LED (CoolLED pE300white, power = 8 mW at the sample plane, Andover, UK) via
755 a FITC filter. All images were analysed using the ImageJ software as previously described
756 [113,114,115].

757 **Determination of mutations underpinning resistance to phage**

758 In order to determine the mutations underpinning resistance to phage in bacteria from wells
759 where we measured bacterial growth in the presence of phage, we plated these survivors on
760 LB agar plates, incubated these plates at 37 °C for 24h and shipped the plates to MicrobesNG.
761 MicrobesNG performed DNA isolation and ull genome sequencing using 2×250 bp paired end
762 sequencing with a minimum coverage of 30× on the Illumina HiSeq sequencer. Analysis of the
763 sequenced genomes was performed using the *breseq* pipeline [116].

764

765 **Comparative bacterial and phage transcriptomic analysis**

766 RNA isolation, library preparation, sequencing, and transcriptomic data processing was
767 performed as previously reported [55,117]. Briefly, RNA isolation was performed using the
768 RNeasy Mini kit (QIAGEN), according to the manufacturer's specifications. Bacteria were
769 grown in triplicate for 4h in flasks containing 50 mL LB, or LB containing phage at an MOI of
770 1, or LB containing ciprofloxacin at 0.125× MIC, or LB containing both phage at an MOI of 1
771 and ciprofloxacin at 0.125× MIC. DNA removal during extraction was carried out using RNase-
772 Free DNase I (Qiagen). RNA concentration and quality were measured using Qubit 1.0
773 fluorometer (ThermoFisher Scientific) and 2200 TapeStation (Agilent), respectively, and only
774 samples with an RNA integrity number above 8 were taken forward. Transcript abundance
775 was quantified using Salmon for each gene in all samples. Subsequent differential analysis
776 was performed using DEseq2 in R software to quantify the log2 fold change in transcript reads
777 [117] for each gene and compared across the four different experimental conditions. Significantly
778 differentially expressed genes were defined as having a log2 fold change greater than 1 and
779 a p-value adjusted for false discovery rate of < 0.05 [55]. Gene ontology enrichment analysis
780 was performed using the clusterProfiler package for R [119]. Enrichment in terms belonging to
781 the "Biological Process" ontology was calculated for each treatment comparison, relative to
782 the set of all genes quantified in the experiment, via a one-sided Fisher exact test
783 (hypergeometric test). P values were adjusted for false discovery by using the method of
784 Benjamini and Hochberg [120]. Finally, the lists of significantly enriched terms were simplified to
785 remove redundant terms, as assessed via their semantic similarity to other enriched terms,
786 using clusterProfiler's simplify function.

787 **Statistical non-linear regression model**

788 We developed a statistical non-linear regression model to fit the experimental data in order to
789 estimate treatment output and the associated uncertainty also for treatment conditions that we
790 did not investigate experimentally. Since the distribution of bacterial growth values (in terms
791 of OD_{600}) in the presence of phage was skewed, we fitted our data with a Gamma distribution
792 function. Moreover, to account for inaccuracies in optical density measurements via a plate
793 reader, we assumed any measurement below an optical density of 0.05 to be equal to 'zero'.
794 Hence, the data had a non-trivial number of zero values, which could not be captured by a
795 conventional gamma distribution. To accommodate this, we included a parameter which
796 controls the probability of an experiment returning an optical density equal to zero. This two-
797 part distribution strategy resulted in what is often called a "hurdle model" [121]. This distribution
798 then had three parameters, one that represented the probability of measuring a value of zero,
799 and two representing the gamma distribution, in our case parameterised to have a mean

parameter and a shape parameter. We assumed that these three parameters could change with the antibiotic concentration and with the phage concentration. We also assumed these relationships to be potentially non-linear. In other words, we assumed the probability of observing a value of zero, the average non-zero observation, and the spread of non-zero observations all depended on the antibiotic and phage concentrations in a complex manner. As such, we modelled these parameters using cubic regression tensor product smoothing splines [122,123]. Additionally, the spline knot locations for the two gamma distribution parameters were constrained to only the points where a non-zero observation was made. To fit this model, and estimate the various parameters, including splines, we used Markov Chain Monte Carlo (MCMC), using the brms R package [124], with default options used for the priors. This provided us with posterior distributions for all the unknown parameters, allowing us to make probabilistic statements and provide full uncertainty estimates. To better capture the uneven measurement intervals of empirical data and because we were interested in the relationships between antibiotic and phage concentrations, it was convenient to apply a log2 transform to the antibiotic concentration and a log10 transformation to the phage concentration values. To avoid numerical issues when the antibiotic or phage concentrations were equal to 0, we added a small value to each zero before applying the transformation (0.01 for the antibiotic data, and $1e^{-10}$ for the phage measurement data). The model allowed us to continuously predict bacterial growth in terms of optical density and the associated uncertainty for both treatment concentrations that were experimentally investigated as well as treatment concentrations that were not experimentally investigated.

Data availability

All data generated or analysed during this study are included in this published article and its supplementary information files.

Acknowledgments

This work was supported by the BBSRC through a grant awarded to S.P., K.T.A. and U.L. (BB/V008021/1). S.K. was supported by a QUEX PhD studentship awarded to S.P., M.A.T.B. and K.T.A. KTA and E.B. gratefully acknowledge the financial support of the EPSRC (EP/T017856/1). K.C., K.B. and S.H. were supported by the Defence Science and Technology Laboratory. This project utilised equipment funded by a Wellcome Trust Institutional Strategic Support Fund (WT097835MF), a Wellcome Trust Multi-User Equipment Award (WT101650MA) and a BBSRC LoLa award (BB/K003240/1). The funders had no role in study design, data collection and analysis, decision to publish, or preparation of the manuscript.

Author contributions

Conceptualization, S.P.; methodology, S.K., U.L., E.B. and E.L.A.; formal analysis, S.K., U. L., E.B. and S.P; generation of figures, S.K., U.L., E.B. and S.P; investigation, S.K., U.L., K.C., E.B., E.L.A., P.O.N., A.F., A.A. E.G., S.K., K.B., S.V.H., K.T.A., M.A.T.B. and S.P.; resources, K.T.A., M.A.T.B. and S.P.; data curation, S.K. and S.P., writing – original draft, S.K. and S.P.; writing – review & editing, S.K., U.L., K.C., E.B., E.L.A., P.O.N., A.F., A.A., E.G., S.K., K.B., S.V.H., K.T.A., M.A.T.B. and S.P.; visualization, S.K., U.L. and S.P.; supervision, S.P., M.A.T.B. and K.T.A.; project administration, S.P.; funding acquisition, S.P., M.A.T.B. and K.T.A..

Declaration of interests

We do not have any competing interests.

846 **References**

847 1. Murray, C.J., Ikuta, K.S., Sharara, F., Swetschinski, L., Robles Aguilar, G., Gray, A., Han, C.,
848 Bisignano, C., Rao, P., Wool, E., et al. (2022). Global burden of bacterial antimicrobial
849 resistance in 2019: a systematic analysis. The Lancet *399*, 629–655. 10.1016/S0140-
850 6736(21)02724-0.

851 2. Rhodes, K.A., and Schweizer, H.P. (2016). Antibiotic resistance in Burkholderia species. Drug
852 Resistance Updates *28*, 82–90. 10.1016/j.drup.2016.07.003.

853 3. Mahenthiralingam, E., Urban, T.A., and Goldberg, J.B. (2005). The multifarious, multireplicon
854 *Burkholderia cepacia* complex. Nat Rev Microbiol *3*, 144–156. 10.1038/nrmicro1085.

855 4. Edouard E Galyov, Paul J Brett, and David DeShazer (2010). Molecular insights into
856 *Burkholderia pseudomallei* and *Burkholderia mallei* pathogenesis. Annual Review
857 Microbiology *64*, 495–517. 10.1146/annurev.micro.112408.134030.

858 5. Blair, J.M.A., Webber, M.A., Baylay, A.J., Ogbolu, D.O., and Piddock, L.J.V. (2015). Molecular
859 mechanisms of antibiotic resistance. Nat Rev Microbiol *13*, 42–51. 10.1038/nrmicro3380.

860 6. Y C Foong, Michelle Tan, and Richard S Bradbury (2014). Melioidosis: a review. Rural Remote
861 Health *14*. 10.22605/RRH2763.

862 7. Mankovich, A.G., Maciel, K., Kavanaugh, M., Kistler, E., Muckle, E., and Weingart, C.L. (2023).
863 Phage-antibiotic synergy reduces *Burkholderia cenocepacia* population. BMC Microbiol *23*.
864 10.1186/s12866-022-02738-0.

865 8. Podnecky, N.L., Rhodes, K.A., and Schweizer, H.P. (2015). Efflux pump-mediated drug
866 resistance in Burkholderia. Front Microbiol *6*, 1–25. 10.3389/fmicb.2015.00305.

867 9. Kamal, F., and Dennis, J.J. (2015). *Burkholderia cepacia* complex phage-antibiotic synergy
868 (PAS): Antibiotics stimulate lytic phage activity. Appl Environ Microbiol *81*, 1132–1138.
869 10.1128/AEM.02850-14.

870 10. Trunck, L.A., Propst, K.L., Wuthiekanun, V., Tuanyok, A., Beckstrom-Sternberg, S.M.,
871 Beckstrom-Sternberg, J.S., Peacock, S.J., Keim, P., Dow, S.W., and Schweizer, H.P. (2009).
872 Molecular basis of rare aminoglycoside susceptibility and pathogenesis of *Burkholderia*
873 *pseudomallei* clinical isolates from Thailand. PLoS Negl Trop Dis *3*, e519.
874 10.1371/journal.pntd.0000519.

875 11. Vaz, A., Burzell, C., Satterwhite, E., Frank, G., Anderson, J., Larsen, J., Billington, J., Shultz, K.,
876 Peers, K., Gitzinger, M., et al. (2020). AMR-2020-Progress-Report. 30–45.

877 12. Czaplewski, L., Bax, R., Clokie, M., Dawson, M., Fairhead, H., Fischetti, V.A., Foster, S.,
878 Gilmore, B.F., Hancock, R.E.W., Harper, D., et al. (2016). Alternatives to antibiotics-a pipeline
879 portfolio review. Lancet Infect Dis *16*, 239–251. 10.1016/S1473-3099(15)00466-1.

880 13. Vidal-Cortés, P., Martin-Loeches, I., Rodríguez, A., Bou, G., Cantón, R., Diaz, E., De la Fuente,
881 C., Torre-Cisneros, J., Nuvials, F.X., Salavert, M., et al. (2022). Current Positioning against
882 Severe Infections Due to *Klebsiella pneumoniae* in Hospitalized Adults. Antibiotics *11*, 1160.
883 10.3390/antibiotics11091160.

884 14. Yang, Y., Guo, Y., Yin, D., Zheng, Y., Wu, S., Zhu, D., and Hu, F. (2021). In vitro activity of
885 cefepime-zidebactam, ceftazidime-avibactam, and other comparators against clinical isolates

886 of enterobacterales, *Pseudomonas aeruginosa*, and *Acinetobacter baumannii*: Results from
887 China antimicrobial surveillance network (CHINET) in 2018. Antimicrob Agents Chemother *65*.
888 10.1128/AAC.01726-20.

889 15. Wiersinga, W.J., Virk, H.S., Torres, A.G., Currie, B.J., Peacock, S.J., Dance, D.A.B., and
890 Limmathurotsakul, D. (2018). Melioidosis. Nat Rev Dis Primers *4*. 10.1038/nrdp.2017.107.

891 16. Worthington, R.J., and Melander, C. (2013). Combination approaches to combat multidrug-
892 resistant bacteria. Trends Biotechnol *31*, 177–184. 10.1016/j.tibtech.2012.12.006.

893 17. Mitchison, D., and Davies, G. (2012). The chemotherapy of tuberculosis: Past, present and
894 future. International Journal of Tuberculosis and Lung Disease *16*, 724–732.
895 10.5588/ijtld.12.0083.

896 18. Kanj, S.S., Bassetti, M., Kiratisin, P., Rodrigues, C., Villegas, M.V., Yu, Y., and van Duin, D.
897 (2022). Clinical data from studies involving novel antibiotics to treat multidrug-resistant
898 Gram-negative bacterial infections. Int J Antimicrob Agents *60*.
899 10.1016/j.ijantimicag.2022.106633.

900 19. Barnes, K.B., Richards, M.I., Burgess, G., Armstrong, S.J., Bentley, C., Maishman, T.C., Laws,
901 T.R., Nelson, M., and Harding, S. V. (2022). Investigation of a combination therapy approach
902 for the treatment of melioidosis. Front Microbiol *13*. 10.3389/fmicb.2022.934312.

903 20. van Heuvel, L., Caini, S., Dückers, M.L.A., and Paget, J. (2022). Assessment of the inclusion of
904 vaccination as an intervention to reduce antimicrobial resistance in AMR national action
905 plans: a global review. Global Health *18*. 10.1186/s12992-022-00878-6.

906 21. Piyush Baindara, and Santi M Manda (2019). Antimicrobial Peptides and Vaccine
907 Development to Control Multi-drug Resistant Bacteria. Protein Pept Lett . *26*, 324–331.

908 22. Yang, S.C., Lin, C.H., Sung, C.T., and Fang, J.Y. (2014). Antibacterial activities of bacteriocins:
909 Application in foods and pharmaceuticals. Front Microbiol *5*, 241. 10.3389/fmicb.2014.00241.

910 23. Goren, M., Yosef, I., and Qimron, U. (2017). Sensitizing pathogens to antibiotics using the
911 CRISPR-Cas system. Drug Resistance Updates *30*, 1–6. 10.1016/j.drup.2016.11.001.

912 24. Wang, C.H., Hsieh, Y.H., Powers, Z.M., and Kao, C.Y. (2020). Defeating antibiotic-resistant
913 bacteria: Exploring alternative therapies for a post-antibiotic era. Int J Mol Sci *21*, 1061.
914 10.3390/ijms21031061.

915 25. Rosini, R., Nicchi, S., Pizza, M., and Rappuoli, R. (2020). Vaccines Against Antimicrobial
916 Resistance. Front Immunol *11*, 1048. 10.3389/fimmu.2020.01048.

917 26. Wu, Y., Battalapalli, D., Hakeem, M.J., Selamneni, V., Zhang, P., Draz, M.S., and Ruan, Z.
918 (2021). Engineered CRISPR-Cas systems for the detection and control of antibiotic-resistant
919 infections. J Nanobiotechnology *19*, 401. 10.1186/s12951-021-01132-8.

920 27. Behrens, H.M., Six, A., Walker, D., and Kleanthous, C. (2017). The therapeutic potential of
921 bacteriocins as protein antibiotics. Emerg Top Life Sci *1*, 65–74. 10.1042/ETLS20160016.

922 28. Strathdee, S.A., Hatfull, G.F., Mutalik, V.K., and Schooley, R.T. (2023). Phage therapy: From
923 biological mechanisms to future directions. Cell *186*, 17–31. 10.1016/j.cell.2022.11.017.

924 29. Kortright, K.E., Chan, B.K., Koff, J.L., and Turner, P.E. (2019). Phage Therapy: A Renewed
925 Approach to Combat Antibiotic-Resistant Bacteria. Cell Host Microbe *25*, 219–232.
926 10.1016/j.chom.2019.01.014.

927 30. Tagliaferri, T.L., Jansen, M., and Horz, H.P. (2019). Fighting Pathogenic Bacteria on Two
928 Fronts: Phages and Antibiotics as Combined Strategy. Front Cell Infect Microbiol *9*.
929 10.3389/fcimb.2019.00022.

930 31. Martin, I., Morales, S., Alton, E.W.F.W., and Davies, J.C. (2023). Lytic Bacteriophage Is a
931 Promising Adjunct to Common Antibiotics across Cystic Fibrosis Clinical Strains and Culture
932 Models of *Pseudomonas aeruginosa* Infection. Antibiotics *12*, 593.
933 10.3390/antibiotics12030593.

934 32. Van Nieuwenhuyse, B., Van der Linden, D., Chatzis, O., Lood, C., Wagemans, J., Lavigne, R.,
935 Schroven, K., Paeshuyse, J., de Magnée, C., Sokal, E., et al. (2022). Bacteriophage-antibiotic
936 combination therapy against extensively drug-resistant *Pseudomonas aeruginosa* infection to
937 allow liver transplantation in a toddler. Nat Commun *13*. 10.1038/s41467-022-33294-w.

938 33. Jones, J.D., Trippett, C., Suleman, M., Clokie, M.R.J., and Clark, J.R. (2023). The Future of
939 Clinical Phage Therapy in the United Kingdom. Viruses *15*, 721. 10.3390/v15030721.

940 34. Krueger, A.P., Col-In, T., Smith, P.N., and Mcguire, C.D. (1948). Observations on the effect of
941 penicillin on the reaction between phage and staphylococci. J Gen Physiol *31*, 477–488.
942 10.1085/jgp.31.6.477.

943 35. Price, W.H. (1947). Bacteriophage formation without bacterial growth; the effect of
944 iodoacetate, fluoride, gramicidin, and azide on the formation of bacteriophage. J Gen Physiol
945 *31*, 135–139. 10.1085/jgp.31.2.135.

946 36. Hadas, H., Einav, M., Fishov, L., and Zaritsky, A. (1997). Bacteriophage T4 development
947 depends on the physiology of its host *Escherichia coli*. Microbiology (N Y) *143*, 179–180.

948 37. Comeau, A.M., Tétart, F., Trojet, S.N., Prère, M.F., and Krisch, H.M. (2007). Phage-antibiotic
949 synergy (PAS): β-lactam and quinolone antibiotics stimulate virulent phage growth. PLoS One
950 *2*. 10.1371/journal.pone.0000799.

951 38. Kamal, F., and Dennis, J.J. (2015). Burkholderia cepacia complex phage-antibiotic synergy
952 (PAS): Antibiotics stimulate lytic phage activity. Appl Environ Microbiol *81*, 1132–1138.
953 10.1128/AEM.02850-14.

954 39. Knezevic, P., Curcin, S., Aleksic, V., Petrusic, M., and Vlaski, L. (2013). Phage-antibiotic
955 synergism: A possible approach to combatting *Pseudomonas aeruginosa*. Res Microbiol *164*,
956 55–60. 10.1016/j.resmic.2012.08.008.

957 40. Ryan, E.M., Alkawareek, M.Y., Donnelly, R.F., and Gilmore, B.F. (2012). Synergistic phage-
958 antibiotic combinations for the control of *Escherichia coli* biofilms in vitro. FEMS Immunol
959 Med Microbiol *65*, 395–398. 10.1111/j.1574-695X.2012.00977.x.

960 41. Kaur, S., Harjai, K., and Chhibber, S. (2012). Methicillin-resistant *Staphylococcus aureus* phage
961 plaque size enhancement using sublethal concentrations of antibiotics. Appl Environ
962 Microbiol *78*, 8227–8233. 10.1128/AEM.02371-12.

963 42. Al-Anany, A.M., Fatima, R., and Hynes, A.P. (2021). Temperate phage-antibiotic synergy
964 eradicates bacteria through depletion of lysogens. Cell Rep *35*, 109–172.
965 10.1016/j.celrep.2021.109172.

966 43. Górski, A., Międzybrodzki, R., Węgrzyn, G., Jończyk-Matysiak, E., Borysowski, J., and Weber-
967 Dąbrowska, B. (2020). Phage therapy: Current status and perspectives. Med Res Rev *40*, 459–
968 463. 10.1002/med.21593.

969 44. Cooper, C.J., Koonjan, S., and Nilsson, A.S. (2018). Enhancing whole phage therapy and their
970 derived antimicrobial enzymes through complex formulation. Pharmaceuticals *11*.
971 10.3390/ph11020034.

972 45. Berryhill, B.A., Huseby, D.L., Mccall, I.C., Hughes, D., and Levin, B.R. (2021). Evaluating the
973 potential efficacy and limitations of a phage for joint antibiotic and phage therapy of
974 *Staphylococcus aureus* infections. PNAS *118*, 118. 10.1073/pnas.2008007118.

975 46. Liu, C.G., Green, S.I., Min, L., Clark, J.R., Salazar, K.C., Terwilliger, A.L., Kaplan, H.B., Trautner,
976 B.W., Ramig, R.F., and Maresso, A.W. (2020). Phage-antibiotic synergy is driven by a unique
977 combination of antibacterial mechanism of action and stoichiometry. mBio *11*, 1–19.
978 10.1128/mBio.01462-20.

979 47. Shan, J., Korbsrisate, S., Withatanung, P., Adler, N.L., Clokie, M.R.J., and Galyov, E.E. (2014).
980 Temperature dependent bacteriophages of a tropical bacterial pathogen. Front Microbiol *5*.
981 10.3389/fmicb.2014.00599.

982 48. Gatedee, J., Kritsiriwuthinan, K., Galyov, E.E., Shan, J., Dubinina, E., Intarak, N., Clokie, M.R.,
983 and Korbsrisate, S. (2011). Isolation and characterization of a novel podovirus which infects
984 *Burkholderia pseudomallei*. Virol J *8*, 366. 10.1186/1743-422X-8-366.

985 49. Lim, Y.M., Vadivelu, J., Mariappan, V., Venkatraman, G., and Vellasamy, K.M. (2023). Effective
986 Therapeutic Options for Melioidosis: Antibiotics versus Phage Therapy. Pathogens *12*.
987 10.3390/pathogens12010011.

988 50. Egilmez, H.I., Morozov, A.Y., Clokie, M.R.J., Shan, J., Letarov, A., and Galyov, E.E. (2018).
989 Temperature-dependent virus lifecycle choices may reveal and predict facets of the biology
990 of opportunistic pathogenic bacteria. Sci Rep *8*. 10.1038/s41598-018-27716-3.

991 51. Attrill, E.L., Claydon, R., Łapińska, U., Recker, M., Meaden, S., Brown, A.T., Westra, E.R.,
992 Harding, S. V., and Pagliara, S. (2021). Individual bacteria in structured environments rely on
993 phenotypic resistance to phage. PLoS Biol *19*. 10.1371/journal.pbio.3001406.

994 52. Łapińska, U., Voliotis, M., Lee, K.K., Campey, A., Stone, M.R.L., Tuck, B., Phetsang, W., Zhang,
995 B., Tsaneva-Atanasova, K., Blaskovich, M.A., et al. (2022). Fast bacterial growth reduces
996 antibiotic accumulation and efficacy. Elife *11*. 10.7554/eLife.74062.

997 53. Hamad, M.A., Di Lorenzo, F., Molinaro, A., and Valvano, M.A. (2012). Aminoarabinose is
998 essential for lipopolysaccharide export and intrinsic antimicrobial peptide resistance in
999 *Burkholderia cenocepacia*. Mol Microbiol *85*, 962–974. 10.1111/j.1365-2958.2012.08154.x.

1000 54. Smith, A., Kaczmar, A., Bamford, R.A., Smith, C., Frustaci, S., Kovacs-Simon, A., O'Neill, P.,
1001 Moore, K., Paszkiewicz, K., Titball, R.W., et al. (2018). The culture environment influences
1002 both gene regulation and phenotypic heterogeneity in *Escherichia coli*. Front Microbiol *9*.
1003 10.3389/fmicb.2018.01739.

1004 55. Glover, G., Voliotis, M., Łapińska, U., Invergo, B.M., Soanes, D., O'Neill, P., Moore, K., Nikolic,
1005 N., Petrov, P.G., Milner, D.S., et al. (2022). Nutrient and salt depletion synergistically boosts
1006 glucose metabolism in individual *Escherichia coli* cells. Commun Biol *5*. 10.1038/s42003-022-
1007 03336-6.

1008 56. Brandão, A.C., Putzeys, L., Pires, D.P., Voet, M., Paeshuyse, J., Azeredo, J., and Lavigne, R.
1009 (2023). Impact of phage predation on *Pseudomonas aeruginosa* adhered to human airway
1010 epithelium: major transcriptomic changes in metabolism and virulence-associated genes.
1011 RNA Biol *20*, 235–247. 10.1080/15476286.2023.2216065.

1012 57. Goode, O., Smith, A., Łapińska, U., Bamford, R., Kahveci, Z., Glover, G., Attrill, E., Carr, A.,
1013 Metz, J., and Pagliara, S. (2021). Heterologous Protein Expression Favors the Formation of
1014 Protein Aggregates in Persister and Viable but Nonculturable Bacteria. ACS Infect Dis *7*, 1848–
1015 1858. 10.1021/acsinfecdis.1c00154.

1016 58. Zhang, Y., Kepiro, I., Ryadnov, M.G., and Pagliara, S. (2023). Single Cell Killing Kinetics
1017 Differentiate Phenotypic Bacterial Responses to Different Antibacterial Classes. Microbiol
1018 Spectr *11*. 10.1128/spectrum.03667-22.

1019 59. Cutts, E.E., Barry Egan, J., Dodd, I.B., and Shearwin, K.E. (2020). A quantitative binding model
1020 for the Apl protein, the dual purpose recombination-directionality factor and lysis-lysogeny
1021 regulator of bacteriophage 186. Nucleic Acids Res *48*, 8914–8926. 10.1093/nar/gkaa655.

1022 60. Bernheim, A., and Sorek, R. (2020). The pan-immune system of bacteria: antiviral defence as
1023 a community resource. Nat Rev Microbiol *18*, 113–119. 10.1038/s41579-019-0278-2.

1024 61. Doron, S., Melamed, S., Ofir, G., Leavitt, A., Lopatina, A., Keren, M., Amitai, G., and Sorek, R.
1025 (2018). Systematic discovery of antiphage defense systems in the microbial pangenome.
1026 Science (1979) *359*. 10.1126/science.aar4120.

1027 62. Wendling, C.C., Lange, J., Liesegang, H., Sieber, M., Pöhlein, A., Bunk, B., Rajkov, J., Goehlich,
1028 H., Roth, O., and Brockhurst, M.A. (2022). Higher phage virulence accelerates the evolution of
1029 host resistance. Proceedings of the Royal Society B: Biological Sciences *289*.
1030 10.1098/rspb.2022.1070.

1031 63. van Houte, S., Buckling, A., and Westra, E.R. (2016). Evolutionary Ecology of Prokaryotic
1032 Immune Mechanisms. Microbiology and Molecular Biology Reviews *80*, 745–763.
1033 10.1128/mmbr.00011-16.

1034 64. Cote, J.M., and Taylor, E.A. (2017). The glycosyltransferases of LPS core: A review of four
1035 heptosyltransferase enzymes in context. Int J Mol Sci *18*. 10.3390/ijms18112256.

1036 65. Li, H., Liao, T., Debowski, A.W., Tang, H., Stubbs, K.A., Marshall, B.J., and Benghezal, M.
1037 (2016). Lipopolysaccharide Structure and Biosynthesis in *Helicobacter pylori* Australia.
1038 Helicobacter, 445–461. 10.1111/hel.12301.

1039 66. Ge, H., Zhang, K., Gu, D., Chen, X., Wang, X., Li, G., Zhu, H., Chang, Y., Zhao, G., Pan, Z., et al.
1040 (2021). The rfbN gene of *Salmonella typhimurium* mediates phage adsorption by modulating
1041 biosynthesis of lipopolysaccharide. Microbiol Res *250*. 10.1016/j.micres.2021.126803.

1042 67. Warring, S.L., Malone, L.M., Jayaraman, J., Easingwood, R.A., Rigano, L.A., Frampton, R.A.,
1043 Visnovsky, S.B., Addison, S.M., Hernandez, L., Pitman, A.R., et al. (2022). A lipopolysaccharide-

1044 dependent phage infects a pseudomonad phytopathogen and can evolve to evade phage
1045 resistance. Environ Microbiol *24*, 4834–4852. 10.1111/1462-2920.16106.

1046 68. Kim, M., Kim, S., Park, B., and Ryu, S. (2014). Core lipopolysaccharide-specific phage SSU5 as
1047 an auxiliary component of a phage cocktail for Salmonella biocontrol. Appl Environ Microbiol
1048 *80*, 1026–1034. 10.1128/AEM.03494-13.

1049 69. Wright, R.C.T., Friman, V.P., Smith, M.C.M., and Brockhurst, M.A. (2019). Resistance evolution
1050 against phage combinations depends on the timing and order of exposure. mBio *10*.
1051 10.1128/mBio.01652-19.

1052 70. Burmeister, A.R., Fortier, A., Roush, C., Lessing, A.J., Bender, R.G., Barahman, R., Grant, R.,
1053 Chan, B.K., and Turner, P.E. (2020). Pleiotropy complicates a trade-off between phage
1054 resistance and antibiotic resistance. PNAS *117*, 11207–11216. 10.1073/pnas.1919888117.

1055 71. Scholl, D., Adhya, S., and Merril, C. (2005). *Escherichia coli* K1's capsule is a barrier to
1056 bacteriophage T7. Appl Environ Microbiol *71*, 4872–4874. 10.1128/AEM.71.8.4872-
1057 4874.2005.

1058 72. Gong, Q., Wang, X., Huang, H., Sun, Y., Qian, X., Xue, F., Ren, J., Dai, J., and Tang, F. (2021).
1059 Novel Host Recognition Mechanism of the K1 Capsule-Specific Phage of *Escherichia coli*:
1060 Capsular Polysaccharide as the First Receptor and Lipopolysaccharide as the Secondary
1061 Receptor. J Virol *95*. 10.1128/jvi.00920-21.

1062 73. Chantratita, N., Wuthiekanun, V., Boonbumrung, K., Tiyawisutsri, R., Vesaratchavest, M.,
1063 Limmathurotsakul, D., Chierakul, W., Wongratanacheewin, S., Pukritiyakamee, S., White, N.J.,
1064 et al. (2007). Biological relevance of colony morphology and phenotypic switching by
1065 *Burkholderia pseudomallei*. J Bacteriol *189*, 807–817. 10.1128/JB.01258-06.

1066 74. Wikraiphat, C., Saiprom, N., Tandhavanant, S., Heiss, C., Azadi, P., Wongsuvan, G., Tuanyok,
1067 A., Holden, M.T.G., Burtnick, M.N., Brett, P.J., et al. (2015). Colony morphology variation of
1068 *Burkholderia pseudomallei* is associated with antigenic variation and O-polysaccharide
1069 modification. Infect Immun *83*, 2127–2138. 10.1128/IAI.02785-14.

1070 75. Nicholls, P., Clark, J.R., Gu Liu, C., Terwilliger, A., and Maresso, A.W. (2023). Class-Driven
1071 Synergy and Antagonism between a Pseudomonas Phage and Antibiotics. Infect Immun *91*.
1072 10.1128/iai.00065-23.

1073 76. Yeh, P., Tschumi, A.I., and Kishony, R. (2006). Functional classification of drugs by properties
1074 of their pairwise interactions. Nat Genet *38*, 489–494. 10.1038/ng1755.

1075 77. Roemhild, R., Bollenbach, T., and Andersson, D.I. (2022). The physiology and genetics of
1076 bacterial responses to antibiotic combinations. Nat Rev Microbiol *20*, 478–490.
1077 10.1038/s41579-022-00700-5.

1078 78. Chait, R., Craney, A., and Kishony, R. (2007). Antibiotic interactions that select against
1079 resistance. Nature *446*, 668–671. 10.1038/nature05685.

1080 79. Brochado, A.R., Telzerow, A., Bobonis, J., Banzhaf, M., Mateus, A., Selkrig, J., Huth, E., Bassler,
1081 S., Zamarreño Beas, J., Zietek, M., et al. (2018). Species-specific activity of antibacterial drug
1082 combinations. Nature *559*, 259–263. 10.1038/s41586-018-0278-9.

1083 80. Wang, Y., Li, X., Dance, D.A.B., Xia, H., Chen, C., Luo, N., Li, A., Li, Y., Zhu, Q., Sun, Q., et al.
1084 (2022). A novel lytic phage potentially effective for phage therapy against *Burkholderia*
1085 *pseudomallei* in the tropics. Infect Dis Poverty *11*. 10.1186/s40249-022-01012-9.

1086 81. Tsunemoto, H., Sugie, J., Enustun, E., Pogliano, K., and Pogliano, J. (2023). Bacterial
1087 cytological profiling reveals interactions between jumbo phage ϕKZ infection and cell wall
1088 active antibiotics in *Pseudomonas aeruginosa*. PLoS One *18*, e0280070.
1089 10.1371/journal.pone.0280070.

1090 82. Liu, D., Van Belleghem, J.D., de Vries, C.R., Burgener, E., Chen, Q., Manasherob, R., Aronson,
1091 J.R., Amanatullah, D.F., Tamma, P.D., and Suh, G.A. (2021). The safety and toxicity of phage
1092 therapy: A review of animal and clinical studies. Viruses *13*. 10.3390/v13071268.

1093 83. Dąbrowska, K., and Abedon, S.T. (2019). Pharmacologically Aware Phage Therapy:
1094 Pharmacodynamic and Pharmacokinetic Obstacles to Phage Antibacterial Action in Animal
1095 and Human Bodies. Microbiology and Molecular Biology Reviews *83*. 10.1128/mmbr.00012-
1096 19.

1097 84. Bulssico, J., Papukashvili, I., Espinosa, L., Gandon, S., and Ansaldi, M. (2022). Phage-antibiotic
1098 synergy: cell filamentation is a key driver of successful phage predation. bioRxiv.
1099 10.1101/2022.11.28.518157.

1100 85. Woods, D.E., Jeddeloh, J.A., Fritz, D.L., and DeShazer, D. (2002). *Burkholderia thailandensis*
1101 E125 harbors a temperate bacteriophage specific for *Burkholderia mallei*. J Bacteriol *184*,
1102 4003–4017. 10.1128/JB.184.14.4003-4017.2002.

1103 86. Wongratanacheewin, S., Nakornpakdee, Y., Sermswan, R.W., Tattawasart, U., Yordpratum, U.,
1104 and Wongratanacheewin, S. (2015). A PCR-based detection of *Burkholderia pseudomallei*
1105 diversity using Myoviridae prophage typing. J trop Med public health *30*.

1106 87. Rhodes, K.A., Somprasong, N., Podnecky, N.L., Mima, T., Chirakul, S., and Schweizer, H.P.
1107 (2018). Molecular determinants of *Burkholderia pseudomallei* BpeEF-OprC efflux pump
1108 expression. Microbiology (United Kingdom) *164*, 1156–1167. 10.1099/mic.0.000691.

1109 88. Krishnamoorthy, G., Weeks, J.W., Zhang, Z., Chandler, C.E., Xue, H., Schweizer, H.P., Ernst,
1110 R.K., and Zgurskaya, H.I. (2019). Efflux Pumps of *Burkholderia thailandensis* Control the
1111 Permeability Barrier of the Outer Membrane. Antimicrob Agents Chemother *63*.
1112 10.1128/AAC.00956-19.

1113 89. Allison, K.R., Brynildsen, M.P., and Collins, J.J. (2011). Metabolite-enabled eradication of
1114 bacterial persisters by aminoglycosides. Nature *473*, 216–220. 10.1038/nature10069.

1115 90. Paulsen, I.T., Brown, M.H., and Skurray, R.A. (1996). Proton-Dependent Multidrug Efflux
1116 Systems. Microbiol Rev *60*, 575–608. 10.1128/mr.60.4.575-608.1996.

1117 91. Le, D., Krasnopeeva, E., Sinjab, F., Pilizota, T., and Kim, M. (2021). Active Efflux Leads to
1118 Heterogeneous Dissipation of Proton Motive Force by Protonophores in Bacteria.
1119 10.1128/mBio.

1120 92. Anes, J., McCusker, M.P., Fanning, S., and Martins, M. (2015). The ins and outs of RND efflux
1121 pumps in *Escherichia coli*. Front Microbiol *6*. 10.3389/fmicb.2015.00587.

1122 93. Griffith, J.M., Basting, P.J., Bischof, K.M., Wrona, E.P., Kunka, K.S., Tancredi, A.C., Moore, J.P.,
1123 Hyman, M.R.L., and Slonczewski, J.L. (2018). Experimental evolution of *Escherichia coli* K-12 in

the presence of proton motive force (PMF) uncoupler carbonyl cyanide m-chlorophenylhydrazone selects for mutations affecting PMF-driven drug efflux pumps. Appl Environ Microbiol *85*. 10.1128/AEM.02792-18.

94. Tamer, Y.T., Gaszek, I., Rodrigues, M., Coskun, F.S., Farid, M., Koh, A.Y., Russ, W., and Toprak, E. (2021). The Antibiotic Efflux Protein TolC Is a Highly Evolvable Target under Colicin E1 or TLS Phage Selection. Mol Biol Evol *38*, 4493–4504. 10.1093/molbev/msab190.

95. Laure, N.N., and Ahn, J. (2022). Phage resistance-mediated trade-offs with antibiotic resistance in *Salmonella typhimurium*. Microb Pathog *171*. 10.1016/j.micpath.2022.105732.

96. Hampton, H.G., Watson, B.N.J., and Fineran, P.C. (2020). The arms race between bacteria and their phage foes. Nature *577*, 327–336. 10.1038/s41586-019-1894-8.

97. Chevallereau, A., Pons, B.J., van Houte, S., and Westra, E.R. (2022). Interactions between bacterial and phage communities in natural environments. Nat Rev Microbiol *20*, 49–62. 10.1038/s41579-021-00602-y.

98. Brendan J M Bohannan, and Richard E Lenski (2000). Linking genetic change to community evolution: Insights from studies of bacteria and bacteriophage. Ecology Letters *3*, 326–3. 10.1046/j.1461-0248.2000.00161.x.

99. Koskella, B., and Brockhurst, M.A. (2014). Bacteria-phage coevolution as a driver of ecological and evolutionary processes in microbial communities. FEMS Microbiol Rev *38*, 916–931. 10.1111/1574-6976.12072.

100. Koonin, E. V., Senkevich, T.G., and Dolja, V. V. (2006). The ancient virus world and evolution of cells. Biol Direct *1*. 10.1186/1745-6150-1-29.

101. Torres-Barceló, C., and Hochberg, M.E. (2016). Evolutionary Rationale for Phages as Complements of Antibiotics. Trends Microbiol *24*, 249–256. 10.1016/j.tim.2015.12.011.

102. Dimitriu, T., Kurilovich, E., Łapińska, U., Severinov, K., Pagliara, S., Szczelkun, M.D., and Westra, E.R. (2022). Bacteriostatic antibiotics promote CRISPR-Cas adaptive immunity by enabling increased spacer acquisition. Cell Host Microbe *30*, 31-40.e5. 10.1016/j.chom.2021.11.014.

103. Kropinski, A.M., Mazzocco, A., Waddell, T.E., Lingohr, E., and Johnson, R.P. (2009). Enumeration of bacteriophages by double agar overlay plaque assay. In Methods in Molecular Biology (Springer), pp. 69–76. 10.1007/978-1-60327-164-6_7.

104. Wiegand, I., Hilpert, K., and Hancock, R.E.W. (2008). Agar and broth dilution methods to determine the minimal inhibitory concentration (MIC) of antimicrobial substances. Nat Protoc *3*, 163–175. 10.1038/nprot.2007.521.

105. Jehangir Cama, and Stefano Pagliara (2020). Microfluidic Single-Cell Phenotyping of the Activity of Peptide-Based Antimicrobials. In Methods in Molecular Biology, pp. 237–253. 10.1007/978-1-0716-0928-6_16.

106. Cama, J., Al Nahas, K., Fletcher, M., Hammond, K., Ryadnov, M.G., Keyser, U.F., and Pagliara, S. (2022). An ultrasensitive microfluidic approach reveals correlations between the physico-chemical and biological activity of experimental peptide antibiotics. Sci Rep *12*. 10.1038/s41598-022-07973-z.

107. Bamford, R.A., Smith, A., Metz, J., Glover, G., Titball, R.W., and Pagliara, S. (2017). Investigating the physiology of viable but non-culturable bacteria by microfluidics and time-lapse microscopy. BMC Biol *15*. 10.1186/s12915-017-0465-4.

108. Pagliara, S., Chimerel, C., Langford, R., Aarts, D.G.A.L., and Keyser, U.F. (2011). Parallel sub-micrometre channels with different dimensions for laser scattering detection. Lab Chip *11*, 3365–3368. 10.1039/c1lc20399a.

109. Łapińska, U., Glover, G., Kahveci, Z., Irwin, N.A.T., Milner, D.S., Tourte, M., Albers, S.V., Santoro, A.E., Richards, T.A., and Pagliara, S. (2023). Systematic comparison of unilamellar vesicles reveals that archaeal core lipid membranes are more permeable than bacterial membranes. PLoS Biol *21*. 10.1371/journal.pbio.3002048.

110. Dettmer, S.L., Keyser, U.F., and Pagliara, S. (2014). Local characterization of hindered Brownian motion by using digital video microscopy and 3D particle tracking. Rev Sci Instrum *85*, 023708. 10.1063/1.4865552.

111. Stone, M.R.L., Łapińska, U., Pagliara, S., Masi, M., Blanchfield, J.T., Cooper, M.A., and Blaskovich, M.A.T. (2020). Fluorescent macrolide probes – synthesis and use in evaluation of bacterial resistance. RSC Chem Biol *1*, 395-404, 10.1039/D0CB00118J.

112 Cama, J., Voliotis, M., Metz, J., Smith, A., Iannucci, J., Keyser, U.F., Tsaneva-Atanasova, K., Pagliara, S., Lab Chip *20*, 2765-2775, 10.1039/D0LC00242A.

113. Łapińska, U., Glover, G., Capilla-Lasheras, P., Young, A.J., and Pagliara, S. (2019). Bacterial ageing in the absence of external stressors. Philosophical Transactions of the Royal Society B: Biological Sciences *374*. 10.1098/rstb.2018.0442.

114. Smith, A., Metz, J., and Pagliara, S. (2019). MMHelper: An automated framework for the analysis of microscopy images acquired with the mother machine. Sci Rep *9*. 10.1038/s41598-019-46567-0.

115. Attrill, E.L., Łapińska, U., Westra, E.R., Harding, S.V., and Pagliara, S. (2023). Slow growing bacteria survive bacteriophage in isolation. ISME Communications, *3*, 95. 10.1038/s43705-023-00299-5.

116. Deatherage, D.E., and Barrick, J.E. (2014). Identification of mutations in laboratory-evolved microbes from next-generation sequencing data using breseq. Methods in Molecular Biology *1151*, 165–188. 10.1007/978-1-4939-0554-6_12.

117. Goode, O., Smith, A., Zarkan, A., Cama, J., Invergo, B.M., Belgami, D., Caño-Muñiz, S., Metz, J., Jeffries, A., Norville, I.H., et al. (2021). Persister *Escherichia coli* Cells Have a Lower Intracellular pH than Susceptible Cells but Maintain Their pH in Response to Antibiotic Treatment. 10.1128/mBio.00909-21.

118. Love, M.I., Huber, W., and Anders, S. (2014). Moderated estimation of fold change and dispersion for RNA-seq data with DESeq2. Genome Biol *15*. 10.1186/s13059-014-0550-8.

119. Yu, G., Wang, L.G., Han, Y., and He, Q.Y. (2012). ClusterProfiler: An R package for comparing biological themes among gene clusters. OMICS *16*, 284–287. 10.1089/omi.2011.0118.

120. Benjamini, Y., and Hochberg, Y. (1995). Controlling the False Discovery Rate: A Practical and Powerful Approach to Multiple Testing. Journal of the Royal Statistical Society: Series B *57*, 289–300. 10.1111/j.2517-6161.1995.tb02031.x.

121. Hu, M.C., Pavlicova, M., and Nunes, E. V. (2011). Zero-inflated and hurdle models of count data with extra zeros: Examples from an HIV-risk reduction intervention trial. American Journal of Drug and Alcohol Abuse *37*, 367–375. 10.3109/00952990.2011.597280.

122. Chung Gu (2002). Smoothing Spline ANOVA Models SSS. (Springer) 10.1007/978-1-4757-3683-0.

123. Wood, S.N. (2017). P-splines with derivative based penalties and tensor product smoothing of unevenly distributed data. Stat Comput *27*, 985–989. 10.1007/s11222-016-9666-x.

124. Bürkner, P.C. (2017). brms: An R package for Bayesian multilevel models using Stan. J Stat Softw *80*. 10.18637/jss.v080.i01.